Tsunami Forecast Model for Savannah, GA

Elena Tolkova

Contents

List of Figures

List of Tables

Abstract

Based on Method Of Splitting Tsunami (MOST) numerical model, a tsunami Forecast Model has been developed for Savannah, GA, centered onto the shores of Calibogue Sound in the vicinity of Savannah city, to be used with the current operational version of the MOST model (v.2). Another Forecast Model for the same locality, along with a reference inundation

model at higher resolution and larger space coverage were developed, to be used with the latest version of the MOST model (v.4). The models showed robust performance with a number of synthetic events, including extreme scenarios. Simulations of several tsunami events with the two Forecast Models and with the Reference Model are performed and analyzed for the models validation and for the associated hazard assessment. It is expected, that the forecast model for Savannah, GA is able to provide an accurate estimate of a wave arrival time, wave height, and inundation extend in minutes of computational time in advance of a tsunami arrival, should the tsunami happen. The work also highlights the MOST version 4 features and new opportunities for the development of the forecast models.

1 Background and objectives

The National Oceanic and Atmospheric Administration (NOAA) Center for Tsunami, Research (NCTR) at the NOAA Pacific Marine Environmental Laboratory (PMEL) has developed a tsunami forecasting capability for operational use by NOAAs two Tsunami Warning Centers located in Hawaii and Alaska (Titov et al., 2005). The system is designed to efficiently provide basin-wide warning of approaching tsunami waves accurately and quickly. The system, termed Short-term Inundation Forecast of Tsunamis (SIFT), combines real-time tsunami event data with numerical models to produce estimates of tsunami wave arrival times and amplitudes at a coastal community of interest. The SIFT system integrates several key components: deep-ocean observations of tsunamis in real time, a basin-wide pre-computed propagation database of water level and flow velocities based on potential seismic unit sources, an inversion algorithm to refine the tsunami source based on deep-ocean observations during an event, and high-resolution tsunami forecast models termed Standby Inundation Models (SIMs).

Thus this work pursues two major goals. First, to develop a Forecast Model for Savannah, GA to be used with the current operational version of the MOST model (v.2). Second, to develop a Forecast Model for Savannah, GA to be used with the latest version of the MOST model (v.4) and in doing so, to highlight the new version features and new opportunities for the development of the forecast models.

2 Forecast Methodology

The NOAA tsunami forecast system employes the Method of Splitting Tsunami (MOST) numerical model (Titov & Synolakis , 1998), which is a set of code for simulating three processes of tsunami evolution: generation by an earthquake, transoceanic propagation, and inundation of dry land at specific sites.

The forecast is supported by the database of an ocean-wide 24-hour-long simulation of a tsunami wave propagation, for numerous tsunamis generated by hypothetic unit earthquakes covering world-wide subduction zones (Gica et al., 2008). As the tsunami wave propagates across the ocean and reaches tsunameter observation sites, the forecasting system uses a data inversion technique coupled with a pre-computed tsunami generation scenarios to deduce the tsunami source in terms of the database unit earthquakes (Percival et al., 2009). A linear combination of the pre-computed unit tsunamis is then used to determine the offshore tsunami waves and to produce synthetic boundary conditions of water elevation and flow velocities into site-specific forecast models. The main objective of a forecast model is to provide an accurate estimate of a wave arrival time, wave height,

and inundation extend at a particular location in minutes of computational time, in advance of the wave arrival. Previous and present development of forecast models in the Pacific (Titov et al., 2005; Titov, 2009; Tang et al., 2008; Wei et al., 2008) have validated the accuracy and efficiency of each forecast model currently implemented in the real-time tsunami forecast system.

3 Model Development

Each forecast model consists of three nested grids with increasing spatial resolution, referred to as A, B, and C-grids. The outer and the coarser grid A receives its boundary input of water elevation and flow velocities from the pre-computed database, and provides the boundary input of a re-fined (with respect to the database) solution into B grid, which is smaller in extent and finer in resolution. B grid further refined solution provides the boundary input into the finest and smallest of the three C grid. Within C grid, the solution is expected to be accurate enough to match the major features of a tide gauge tsunami record.

All tsunami forecast models are run in real time while a tsunami is propagating across the open ocean. Thus the computational time is the critical factor for a model development. Meeting the time constrain is achieved by manipulating with the spatial and temporal resolution of grids used in modeling, with an objective to balance computational speed with numerical accuracy.

The development of a Forecast Model is centered around "optimizing" (reducing) coverage and resolution of computational grids, to reduce the computational time as much as possible without noticeable degradation of the numerical solution, in particular, a time history at an observational point (usually, at a tide gage location). Time histories computed with optimized grids are evaluated by visual comparison with the time history obtained with a reference model comprised of larger and/or finer grids (Tang et al., 2009).

In this work, the reference model consists of shoreline-oriented grids, and the reference runs were performed with the latest version of the MOST model, namely the version 4. Two optimized models are developed, one utilizing grids in conventional longitude/latitude coordinate system which can be used with any MOST version, and another one utilizing shoreline oriented grids which can be used with the MOST v.4 only.

MOST v.4 is the further development of the "curvilinear MOST" (Tolkova, 2008), previously (but not anymore) being also referred to as MOST v.4. The present MOST v.4 performs computations in nested grids representing points on the Earth surface by zonal and azimuth angles in coordinate systems arbitrary rotated with respect to each other and to the geophysical system (that is, one having longitude and latitude as zonal and azimuth angles). The purpose of the rotation is to aline the grid orientation with local bathymetry features at a certain scale. The technique of grid development in the rotated coordinates is described in (Tolkova, 2008). This technique also results in grids with low values of the azimuth angle ("own latitude"), that is, with a grid's cell shape being as perfectly rectangular as possible on a sphere.

3.1 Forecast Area

The city of Savannah is situated on Savannah river, 15 miles upstream from Calibogue Sound of Atlantic ocean. A tsunami forecast model for Savannah, GA will narrow onto the shores of Calibogue Sound in the vicinity of Savannah city (due to its remoteness from the ocean, the city itself is not in much danger of a tsunami). An area between the city of Savannah and the Atlantic shore includes extended tidal lands, and therefore most of it is not populated. The populated areas

on the Atlantic shore in the vicinity of the city of Savannah are Tybee Island, Daufuskie Island, and Hilton Head Island (Figures 1, 2).

Tybee Island is the easternmost point in the state of Georgia. As of the census of 2000, there were 3392 people, 13.8% under the age of 18.

Daufuskie Island is an 8 square miles residential island between Savannah and Hilton Head Island. It has a full-time population of around 430.

Hilton Head Island features 12 miles (19 km) of beachfront on the Atlantic Ocean. Its full-time population is 34,407 (US census 2000), 17.3% under the age of 18.

The three islands, however, are popular vacation destinations, so the visitors add to the population significantly. For Hilton Head, the year-round population was 75,504 at the 2000 census, although during the peak of summer vacation season the population can swell to 275,000.

The area's tide gage is located in Fort Pulaski National Monument in the mouth of Savannah river, at 32.033333^oN, 80.901667^oW. The tide station in the area was established on July 1, 1935, in the present installation since May 14, 1990. The gage location on a map is shown in Figure 8. There is no record of any actual tsunami in this area.

3.2 Model Setup: Bathymetry sources and grid selection

The forecast model A-grid was cut from East Coast grid with 9 arc-sec resolution, compiled from a variety of sources (NGDC, 2005). No conversion to a common vertical datum was performed, which yields Mean Sea Level as the assumed vertical reference. The grid contains no topography data. B and C grids were cut from Savannah DEM with 1/3 arc-sec resolution referenced to Mean High Water, for modeling of worst-case scenario flooding (Taylor et al., 2006). One meter was added to the A-grid bathymetry (approximately half of the tidal range at the location), to reduce a mismatch between the depths at the same location in A and B grids, noticeable due to small depths on B grid boundary (about 20 m). Both source grids were low-pass filtered to avoid aliasing when re-sampled to desired resolution.

The parameters of the reference, optimized, and some other grids being employed while deciding on the grids' coverage and resolution are given in Table 1, and the grids' coverage is shown in Figures 3, 8. Computational (CPU) times listed in the Table and anywhere in this work were recorded with Dell PowerEdge Linux machine, 2 x 2.66 GHz Xeon X5355 quad-core processors, running MOST code compiled with PGI Fortran compiler.

3.2.1 Selecting A grid

To decide on how the solution in an inner (B) grid is affected by A grid coverage and resolution, boundary inputs into a possible B-gird (not listed in the table 1) were computed with tentative outer grids A1 - A5, for an artificial Mw 8.7 event, originated with unit sources a49-53, b49-53 (Atlantic subduction zone) with a factor 10, and further referred to as grid-test event. Grid A1 has the larger coverage of 4.0 (on-shore) x 6.0 (along-shore) degree of the Great circle, or 445.2 km x 667.8 km, and the finer resolution (30 s). Grids A2 and A3 have the same coverage as A1 and lower resolution of 60 s and 90 s correspondently. Grids A4 and A5 have the smaller coverage of 2.6 (on-shore) x 4.0 (along-shore) degree of the Great circle arc, or 289.4 km x 445.2 km, and resolution of 30 s and 60 s, correspondently. The larger and smaller A-grid areas are shown in Figure 3.

Figure 4 displays boundary time series on the three wet sides of a possible B grid, computed with larger grids A1, A2, A3. Figure 5 displays B-boundary time series computed with grids A1,

Grid name	notes	MOST version	resolution, arc-s azmth (lat)	resolution, arc-s zonal (lon)	row×clm	dt_{max}, s	dt, s	CPU time, min	Smltn time, hours
A1	large	v.4	30	30	481×721	4.83	3.5	18	6
A2	large	v.4	60	60	241×361	9.65	7	2.25	
A3	large	v.4	90	90	161×241	14.48	10	0.8	
A4	opt	v.4	30	30	313×481	9.88	9	6.2	12
A5	small	v.4	60	60	157×241	19.8	15	0.5	6.3
A6	ref	v.4	20	20	721×1081	3.22	3	98	12
B1	ref	v.4	5	5	361×429	9.1	7	8.0	
B2	opt	v.4	10	10	181×215	18.2	15	1	
C1	ref	v.4	0.7	0.7	618×823	1.45	1.2	140	
C2	opt	v.4	2	2	199×289	4.2	3.8	5.0	
A	opt	v.2	30	35.3	433×368	9.5	9	13.8 (v.4)	12
B	opt	v.2	10	11.79	181×211	19.3	12	16.2 (v.2)	
C	opt	v.2	2	2.36	266×245	4.38	3	altogether	

Table 1: The list of the reference, optimized, and some other grids considered for the model development, and their parameters.

A4, A5. Plots of individual time histories at four boundary nodes can be found in Figures 6 and 7.

It can be seen by visual comparison of the results obtained with the grid A1 (the larger and finer grid among the five) and the other grids, that reducing the grid resolution affected the results more than reducing the grid coverage. Using A4 (the smaller 30s grid) gives the results closest to the results for A1 in 1/3 of the computational time (see Table 1), even though it takes ocean-side boundary of grid A from 1000 m to only 500 m depth. Grid A4 is adopted as the optimized grid for the Forecast Model for MOST v.4.

3.2.2 Selecting B-grid

Within the forecast methodology, a purpose of a B grid is to refine an A-grid solution before it goes into a C grid. Thus a C-grid input obtained directly from an A-grid provides the starting point from which refinements are to be made. To visualize those refinements and select a B grid, boundary inputs into C grid were compared, computed directly from optimized A grid (30 s resolution, no topography), and from two possible B grids. The two B grids have the same coverage shown in Figures 3 and 8 (the grid coverage for the v.4 version is the largest possible with the given DEM for the area) and resolutions of 10 s and 5 s. B-grid coverage is 0.5 (on-shore) x 0.6 (along-shore) degree of the Great circle arc, or 55.65 km x 66.78 km.

The area is characterized by extended shallow water and extended tidal lands, that is, very low values for both water depth and land elevation. An average water depth within the C grid is 5.8 m. An average water depth within the B grid is 11.2 m, with the depth on the ocean side boundary being about 20 m. DEM coverage does not allow to extend B grid to greater depth. However, with A grid resolution finer than for the majority of Pacific models (30 s vs. 1-2 min), the area of validity of A grid solution extends shallower, as can be deduced from A-grid solution on C-grid boundary

being very close to the refined (B-grid) solution (Figure 10).

It can be seen in time histories at selected points on C-grid boundary (see Figure 11), that additional scattering on near-shore features accounted for in B grid results in slight reduction in the wave amplitude (later waves especially), though the general wave envelope as it comes from A grid is not much affected. The results for the two B grids of different resolution are practically identical, while the computations with the coarser grid are 8 times faster. The coarser B grid is adopted as the optimized grid for the Forecast Model for MOST v.4.

3.2.3 Selecting C-grid

C-grid coverage for this location was much determined by the physical features, that is, by an objective to include shallow Calibogue Sound entirely. For the reference, the coverage was slightly extended North (see Figures 8, 9). Resolution of 0.7 arc-sec for the reference grid and 2 arc-sec for the optimized grid were considered. As above, a time history obtained directly from B-grid provides the starting point from which refinements are to be made.

Figure 12 displays time histories at an observational point obtained directly from the optimized B-grid and the two C grids. The actual location of the nodes where the two C-grid time series came from is 8.7 m apart form each other and 87 m away from the location where the B-grid time series were read from.

It can be seen, that even B-grid solution provides a time history estimate fairly close to the most refined one (obtained with the finer C-grid), at least for the grid-test event. Time histories obtained with the two C grids are very close, with the computation time being 5 min for the coarser grid and 2 h 20 min for the finer grid. The coarser C grid is adapted as the optimized grid. The grid's coverage is 0.11 (cross-shore) x 0.16 (along-shore) degree of the Great circle arc, or 12.30 km x 17.87 km.

3.2.4 Final selection of the grids for Forecast Models

A set of grids for the reference model is comprised of A grid at 20 arc-sec resolution with the larger coverage, B grid at 5 arc-sec, and C grid at 0.7 arc-sec (grids A6, B1, C1 in Table 1). 12 h simulation in the reference model takes 4.15 hour of computer time.

A set of grids for the optimized model for MOST v.4 is comprised of A grid at 30 arc-sec resolution with the smaller coverage, B grid at 10 arc-sec, and C grid at 2 arc-sec (grids A4, B2, C2 in Table 1). 12 h simulation in the optimized model takes 12 min of computer time.

A set of grids for the optimized model for MOST v.2 was selected with the same resolution and similar coverage as for v.4 optimized model (grids A, B, C in Table 1). To keep a cell shape square, an increment in longitude between a grid' columns is slightly larger, than increment in latitude between the grid rows, as listed in the Table 1. 12 h simulation with Forecast Model for MOST v.2 takes 16.2 min of computer time when run with MOST v.2, and 13.8 min when run with MOST v.4. [1]

The models' parameter files are given in Appendix.

[1] In this particular case, 1/3 of the computational time difference (0.86 min out of 2.4 min) between the versions is due to the fact, that MOST v.4 starts computations in each inner grid as the wave approaches its boundary, while MOST v.2 performs computations in all the grids simultaneously, since the moment a wave touched the boundary of the outer grid A.

4 Results and Discussion

In the next section, the simulations of several tsunami events with the two Forecast Models and with the Reference Model are analyzed for the models validation and for the associated hazard assessment.

4.1 Model Validation

There is no record of an actual tsunami event at the location. To infer on the tsunami behavior and the extent of associated danger, and also to test the model for stability and the two MOST versions for mutual consistence, six artificial mega-events of Mw 9.3 / 9.4 were simulated for 24 h with the both Forecast Models. The events sources were selected to represent different locations within Atlantic (Caribbean) subduction zone, namely AB17-26 with a factor 25 (further referred to as Mega 1), AB35-44 with a factor 25 (Mega 2), AB48-57 with a factor 25 (Mega 3), AB69-78 with a factor 25 (Mega 4), AB82-91 with a factor 30 (Mega 5), and South Sandwich subduction zone AB1-10 with a factor 30 (Mega 6). Location of the unit sources comprising the events in Caribbean basin is shown in Figure 13. The first four events were simulated with the reference model as well. Synthetic scenarios used with the model development and validation are listed in Table 2. Comparison of the results obtained with all the models is presented and discussed below.

Case Name	Sources	Source Zone	Tsunami Source	α (m)
Mega 1	ATSZ 17-26	Atlantic	A17-26, B17-26	25
Mega 2	ATSZ 35-44	Atlantic	A35-44, B35-44	25
Mega 3	ATSZ 48-57	Atlantic	A48-57, B48-57	25
Mega 4	ATSZ 69-78	Atlantic	A69-78, B69-78	25
Mega 5	ATSZ 82-91	Atlantic	A82-91, B82-91	30
Mega 6	SSSZ 1-10	South Sandwich	A1-10, B1-10	30
Grid-test	ATSZ 49-53	Atlantic	A49-53, B49-53	10

Table 2: Synthetic scenarios used with the model development and validation.

Figures 14-25 show time histories at the tide gage location and at another observation point on the ocean side of Tybee island (see Fig.26-31 for the observation points location) computed for the mega events with Forecast Models for MOST v.2 and v.4 and the Reference Model. Figures 14-31 show maximal wave elevation in grid C within 24 h after tsunami generation, computed for the mega events with the three model.

The solutions by the two Forecast Models and the Reference Model are fairly agree with each other. The differences in the results can be attributed to the different resolution and coverage of the three sets of grids. Also, the time histories came from the nodes (closest to the observation point in each C grid) whose locations do not coincide.

For the gage, the time histories came from locations which are 15.7 m apart between Reference and Forecast v.4 Models, 5.2 m apart between Reference and Forecast v.2 Models, 16.9 m apart between Forecast Models v.2 and v.4

For the second observation point, the time histories came from locations which are 27.4 m apart between Reference and Forecast v.4 Models, 11.8 m apart between Reference and Forecast v.2

Models, 36.4 m apart between Forecast Models v.2 and v.4

The difference between the two Forecast Models and the Reference Model represents a measure of an uncertainty in the numerical solution.

As it was expected and the simulation confirmed, the most destructive tsunami came from the Eastern part of Caribbean (Mega 3), where there is unobscured pass for the wave to the Savannah coast. Other tsunami origins in Caribbean are surrounded by islands and other features, which trap most of the wave energy. Consequently, the tsunamis of the same magnitude originated at these locations arrived at Savannah with an amplitude about 3 times smaller than the amplitude of Mega 3 tsunami. Also, the significant part of the tsunami energy comes back to the US East coast after reflecting from Africa. This results in large later waves which could arrive as late as 20 h after the tsunami generation. The largest waves from a tsunami originating in south Sandwich subduction zone arrive 22+ hours after the seismic event.

Events originating in Caribbean caused some inundation of low-laying land, with Mega 3 event causing most extensive inundation affecting populated areas, such as Tybee Island, Daufuskie Landing, and the shores of Hilton Head Island (for the last case, the inundation is simulated for its Southern tip only). Land areas in C grid inundated anytime within 24 h after the tsunami generation in the first four events are shown in Figure 32.

5 Summary and Conclusion

A reference model and two optimized models have been developed for a part of the Atlantic coast in the vicinity of the city of Savannah, GA (Calibogue Sound). The models showed robust performance with a number of synthetic events, including extreme scenarios. In the absence of records of any actual tsunami at the location, the validity of the models is deduced form the following considerations:

- tsunami wave propagation and transformation near land is governed by the same physical laws at any location;
- MOST numerical model has been proved to simulate tsunami propagation and run-up correctly for numerous locations and events throughout the Globe, subject to an accuracy of a numerical set-up;
- the proper choice of the numerical parameters for the Savannah model (such as the model coverage, spatial and temporal resolution) was given full attention to, as described in detail in this report;
- the general wave patterns in the Calibogue Sound and time histories by the coast evaluated at different computational settings (with the reference and the two optimized models different in resolution, spatial extend and the shape of the grids) are consistent with each other, which is a manifestation of the numerical accuracy.

Therefore it is expected, that the forecast model for the Savannah area is able to provide an accurate estimate of a wave arrival time, wave height, and inundation extend in advance of a tsunami arrival, should the tsunami happen. 12 hour simulation of the tsunami propagation and run-up in the area presently requires 12 to 16 min of computational time (Dell Power-Edge Linux computer),

depending on the MOST version employed.

The bathymetry and topography used in the development of this forecast model was based on a digital elevation model provided by the National Geophysical Data Center and the author considers it to be an adequate representation of the local topography/bathymetry. As new digital elevation models become available, forecast models will be updated and report updates will be posted at http://nctr.pmel.noaa.gov/forecast_reports/.

6 Acknowledgments

This work was funded by NOAA/PMEL and by the Joint Institute for the Study of the Atmosphere and Ocean (JISAO) under NOAA Cooperative Agreement No. NA17RJ1232, Contribution .... (JISAO), ... (PMEL).

References

Gica E., Spillane M.C., Titov V.V., Chamberlin C.D. and Newman J.C. (2008): Development of the forecast propagation database for NOAA's Short-Term Inundation Forecast for Tsunamis (SIFT), NOAA Tech. Memo. OAR PMEL-139, 89pp.

National Geophysical Data Center. East coast and Gulf Coast and Caribbean nine second tsunami propagation grids compilation report, 11 pp.
http://onda.pmel.noaa.gov/atlas/citation/10/9sec_intermediate_sub.doc

Percival, D.B., D. Arcas, D.W. Denbo, M.C. Eble, E. Gica, H.O. Mofjeld, M.C. Spillane, L. Tang, and V.V. Titov (2009): Extracting tsunami source parameters via inversion of DART buoy data. NOAA Tech. Memo. OAR PMEL-144, 22 pp.

Savannah Community Profile, 11 pp.
http://savannah.locale.com/GA-orientation/

Tang, L., V.V. Titov, Y. Wei, H.O. Mofjeld, M. Spillane, D. Arcas, E.N. Bernard, C. Chamberlin, E. Gica, and J. Newman (2008): Tsunami forecast analysis for the May 2006 Tonga tsunami. J. Geophys. Res., 113, C12015, doi: 10.1029/2008JC004922.

Tang L., V. V. Titov, and C.D.Chamberlin (2009): Development, testing, and applications of site-specific tsunami inundation models for real-time forecasting. J. Geophys. Res., 6, doi: 10.1029/2009JC005476, in press.

Taylor, L.A., B.W. Eakins, K.S. Carignan, R.R. Warnken, T. Sazonova, D.C. Schoolcraft, and G.F. Sharman (2006): Digital Elevation Model for Savannah, Georgia: Procedures, Data Sources and Analysis. NOAA National Geophysical Data Center (NGDC), 32 pp.
http://onda.pmel.noaa.gov/atlas/citation/33/Savannah.pdf

Titov V. V., González F. I., Bernard E. N., Eble M. C., Mofjeld H. O., Newman J. C., Venturato A. J., 2005. Real - Time Tsunami Forecasting: Challenges and Solutions. Natural Hazards, 35: 41 - 58.

Titov V. V., Synolakis C. E., Numerical Modeling of Tidal Wave Runup, 1998, J. Waterway, Port, Coastal and Ocean Eng., V 124, July / August, N 4, 157 - 171.

Titov, V.V., 2009. Tsunami forecasting. Chapter 12 in The Sea, Volume 15: Tsunamis, Harvard University Press, Cambridge, MA and London, England, 371400.

Tolkova, E (2008). Curvilinear MOST and its first application: Regional Forecast version 2. In: D. Burwell and E. Tolkova. Curvilinear version of the MOST model with application to the coast-wide tsunami forecast. NOAA Tech. Memo. OAR PMEL-142, 28 pp.

Wei, Y., E. Bernard, L. Tang, R. Weiss, V. Titov, C. Moore, M. Spillane, M. Hopkins, and U. Kanoglu (2008): Real-time experimental forecast of the Peruvian tsunami of August 2007 for U.S. coastlines. Geophys. Res. Lett., 35, L04609, doi: 10.1029/2007GL032250.

U.S. Census Bureau. http://www.census.gov

A Reference and optimized model parameters for *.in files, to be used with MOST v.2 and MOST v.4

0.001	Minimum amp. of input offshore wave (m)
1.0	Minimum depth of offshore (m)
0.1	Dry land depth of inundation (m)
0.0009	Friction coefficient (n**2)
1	run up in a and b
300.0	max wave height meters
3	time step (sec)
14400	number of steps for 12 h simulation
3	Compute "A" arrays every n-th time step, n=
4	Compute "B" arrays every n-th time step, n=
24	Input number of steps between snapshots
0	...starting from
1	...saving grid every n-th node, n=

Table 3: Parameters for optimized 12-hour simulation with MOST v.2.

	A ref	B ref	C ref	A opt	B opt	C opt
Min ampl. of input wave (m)	0.005	0.001	0.001	0.005	0.001	0.001
Min depth for offshore (m)	5	1	1	5	1	1
Dry land depth (m)	0.1	0.1	0.1	0.1	0.1	0.1
Friction coefficient (n**2)	0.0009	0.0009	0.0009	0.0009	0.0009	0.0009
number of grids	2	2	1	2	2	1
time step (sec)	3	7	1.2	9	15	3.8
number of steps	14400	6250	35000	4800	3000	11500
grids	A6, B1	B1, C1	C1	A4, B2	B2, C2	C2
0 /runup flag/ 1	0 1 1	0 1 1	0 2 1	0 1 1	0 1 1	0 2 1
steps between snapshots	20	10	50	8	4	10
starting from	0	0	0	0	0	0
saving every n-th node, n=	1	1	2	1	1	1

Table 4: Parameters for reference and optimized 12-hour simulation with MOST v.4. Each grid has a specific set of the parameters.

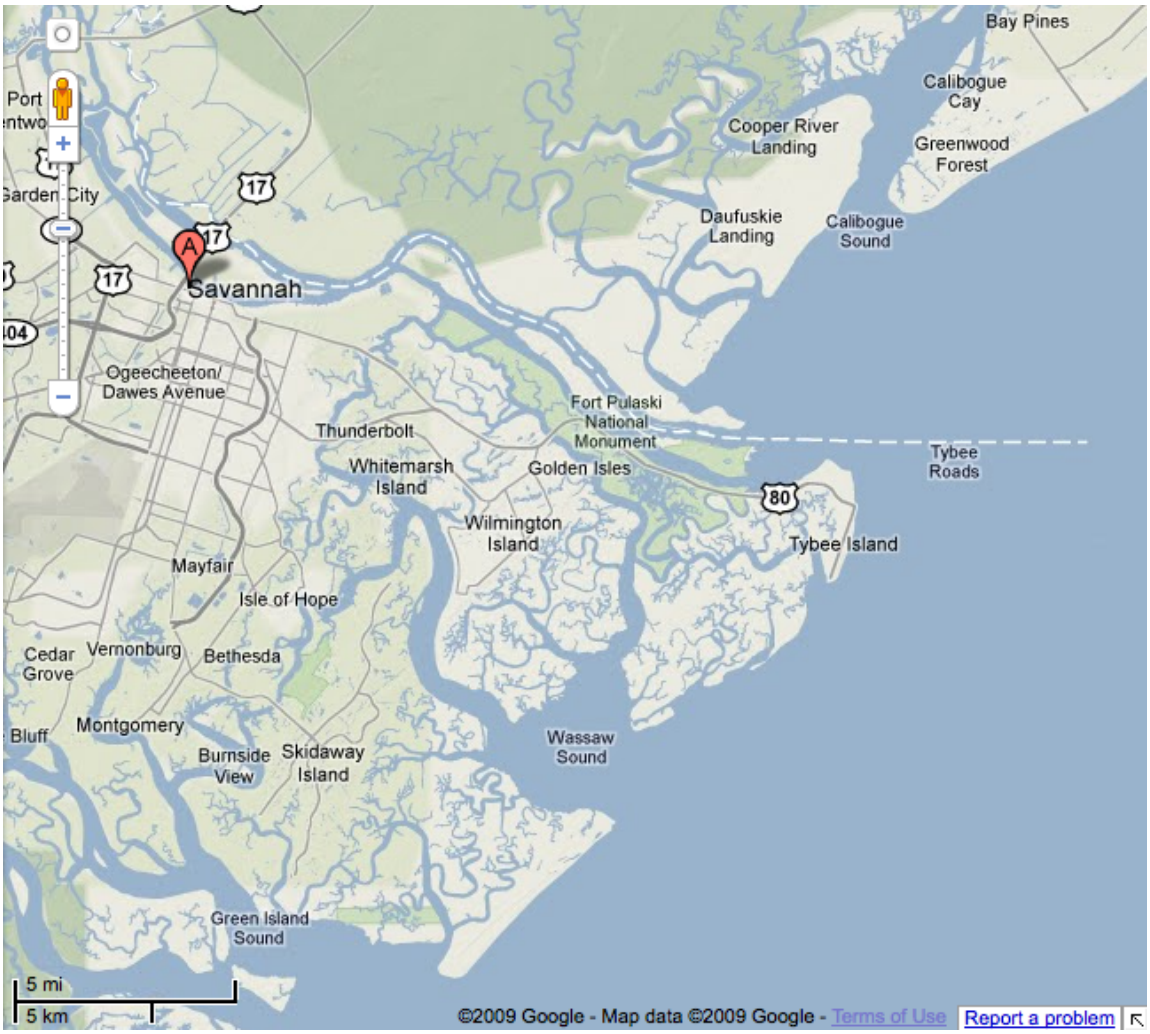

Figure 1: Atlantic vicinity of Savannah on Google Maps.

Figure 2: Air view down to a fractal of streams of the area's Atlantic coast (Savannah Community Profile, 2009).

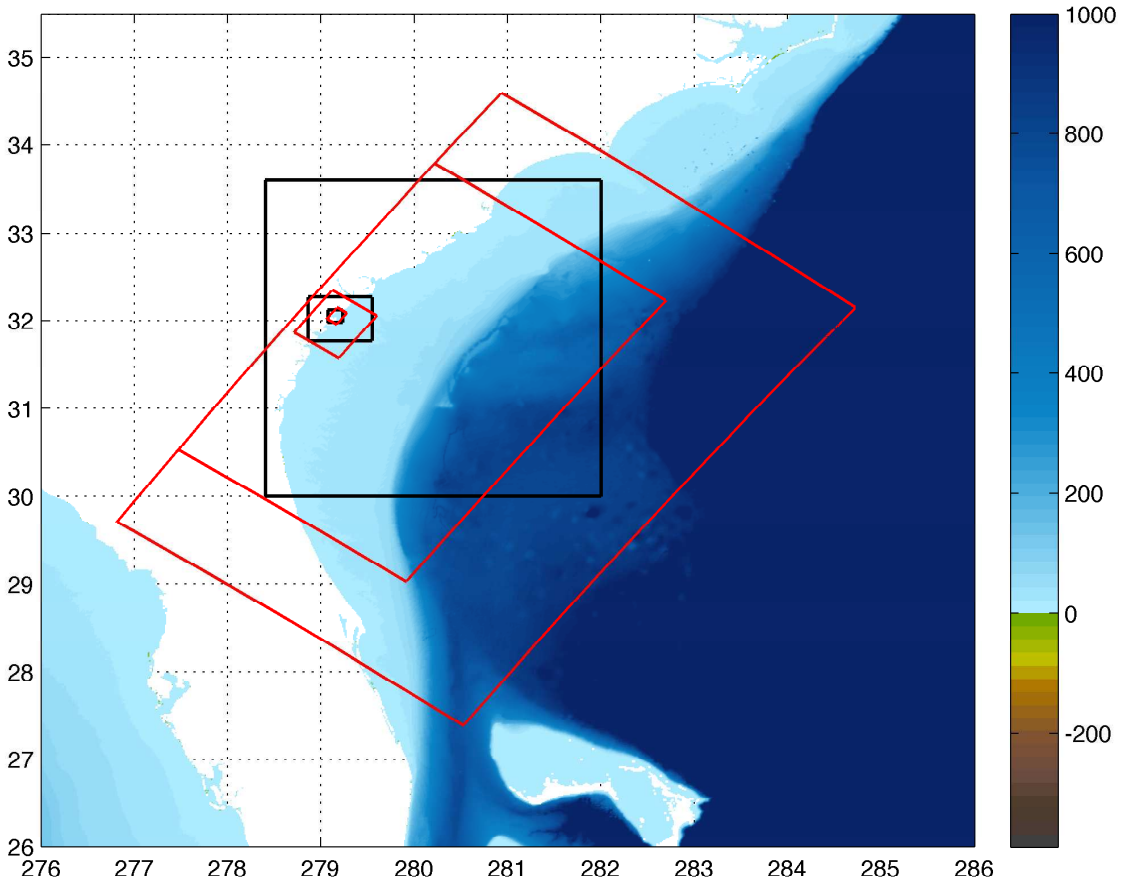

Figure 3: Savannah grids coverage: A reference, A optimized, B, C for v.2 (black) and v.4 (red). X-axis: longitude, degree East, Y-axis - latitude, degree North. Colorscale - meters.

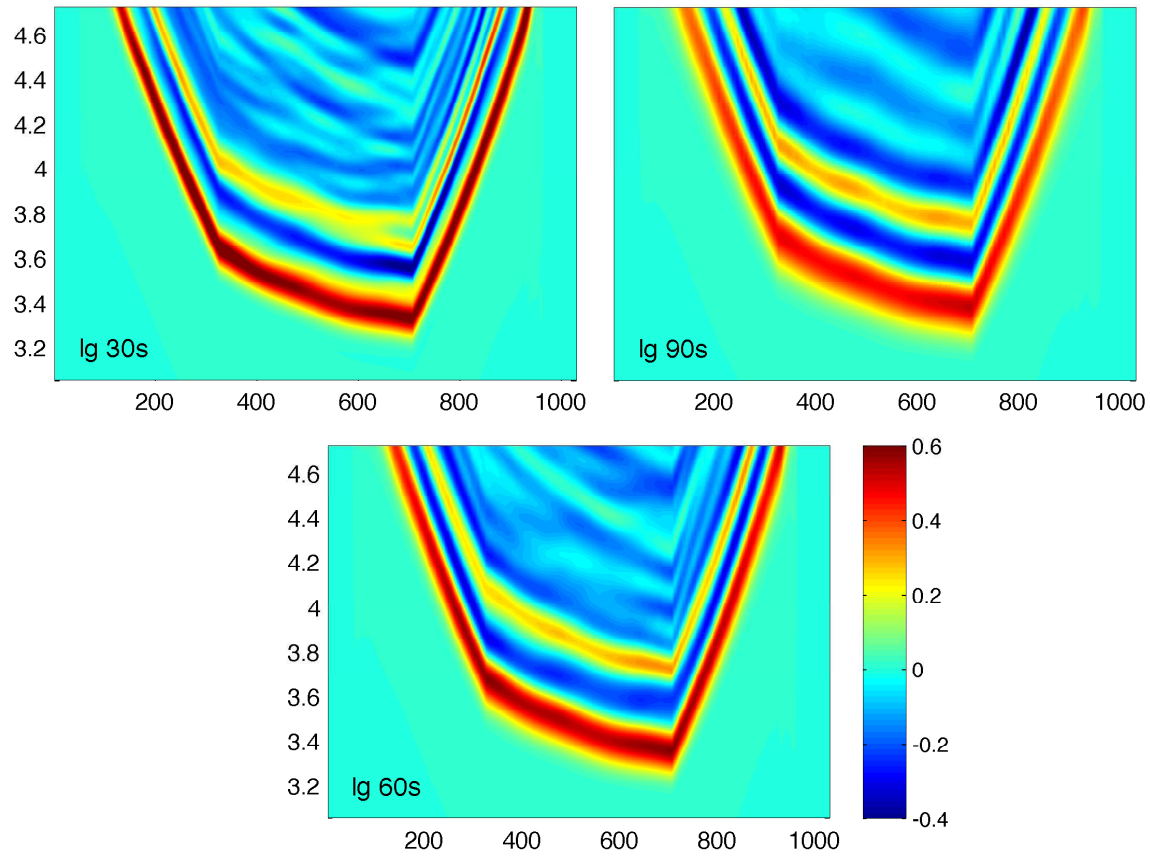

Figure 4: Boundary input into a hypothetical B grid from larger A grid at 30 s, 60 s, 90 s resolution. Y-axis: hour, X-axis: node along the B-boundary, colorscale: meters. Grid-test event.

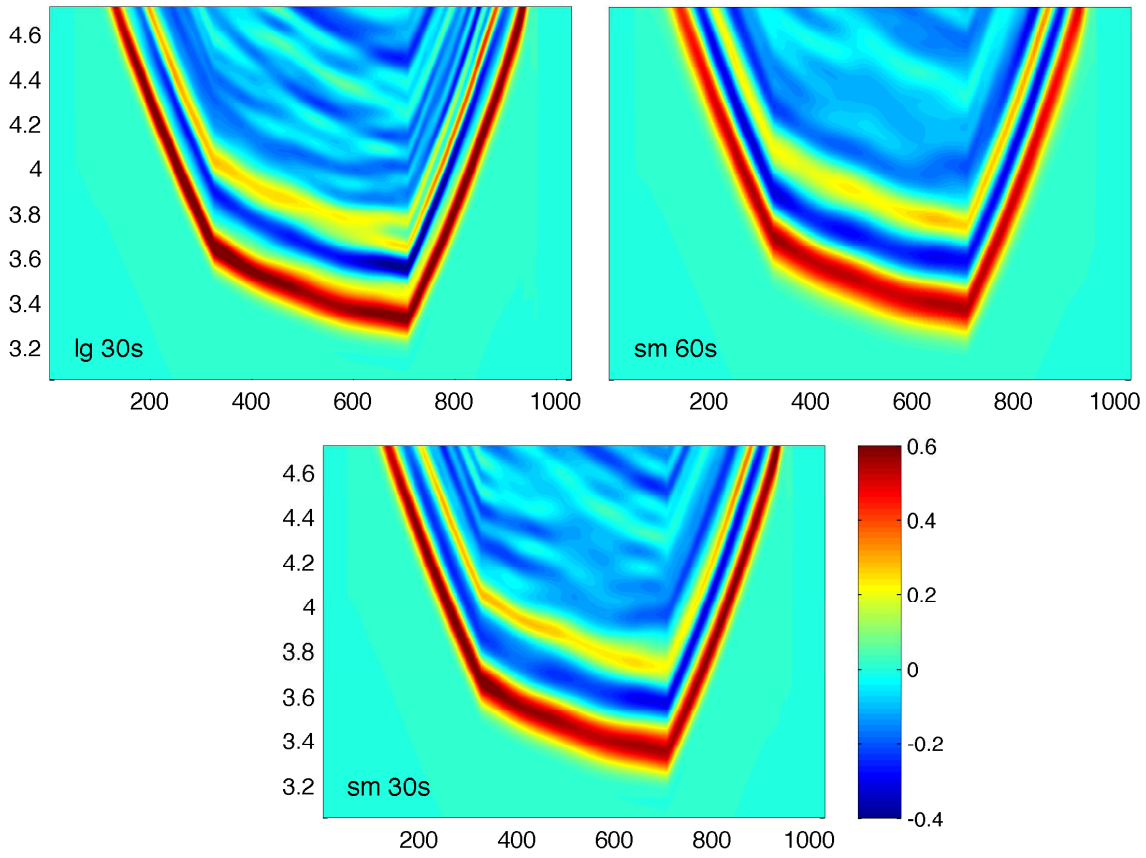

Figure 5: Boundary input into larger B grid from larger A grid at 30 s and smaller A grids at 30 s and 60 s resolution. Y-axis: hour, X-axis: node along the B-boundary, colorscale: meters. Grid-test event.

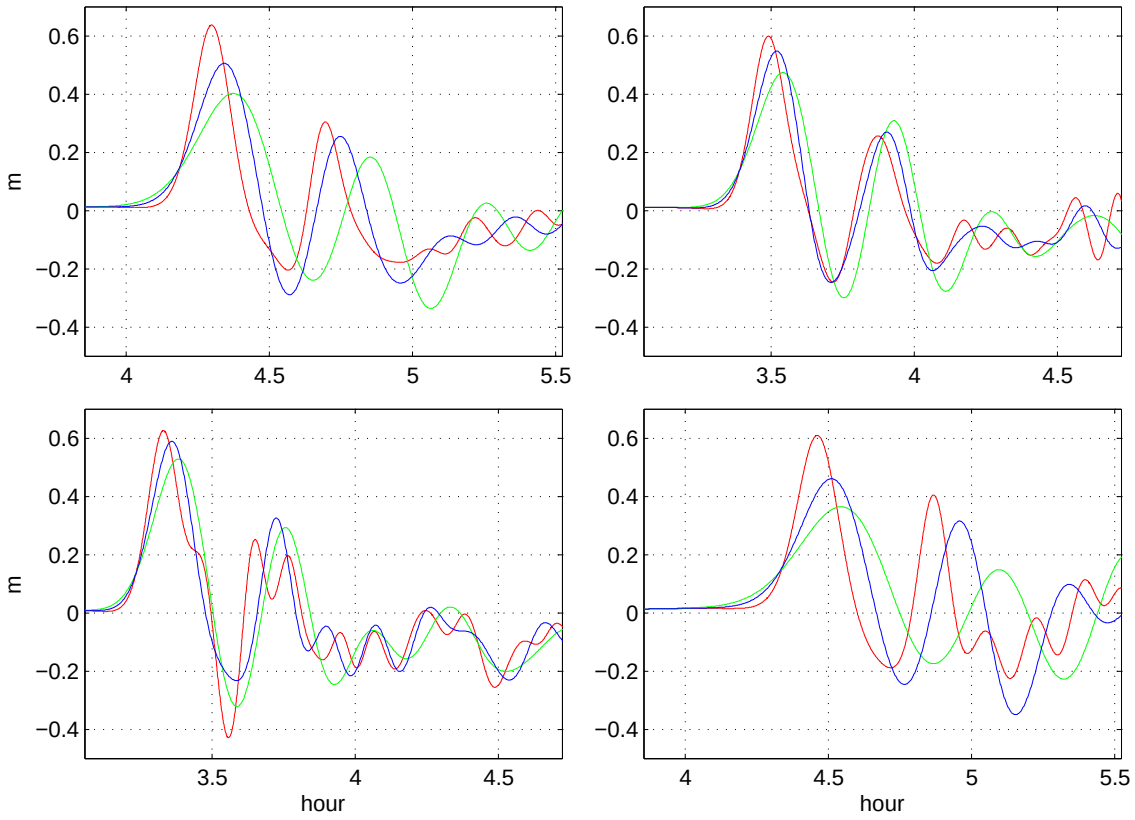

Figure 6: B-boundary timeseries at nodes 200, 450, 700, and 900 from larger A grid at 30 s (red), 60 s (blue), and 90 s (green) resolution. Grid-test event.

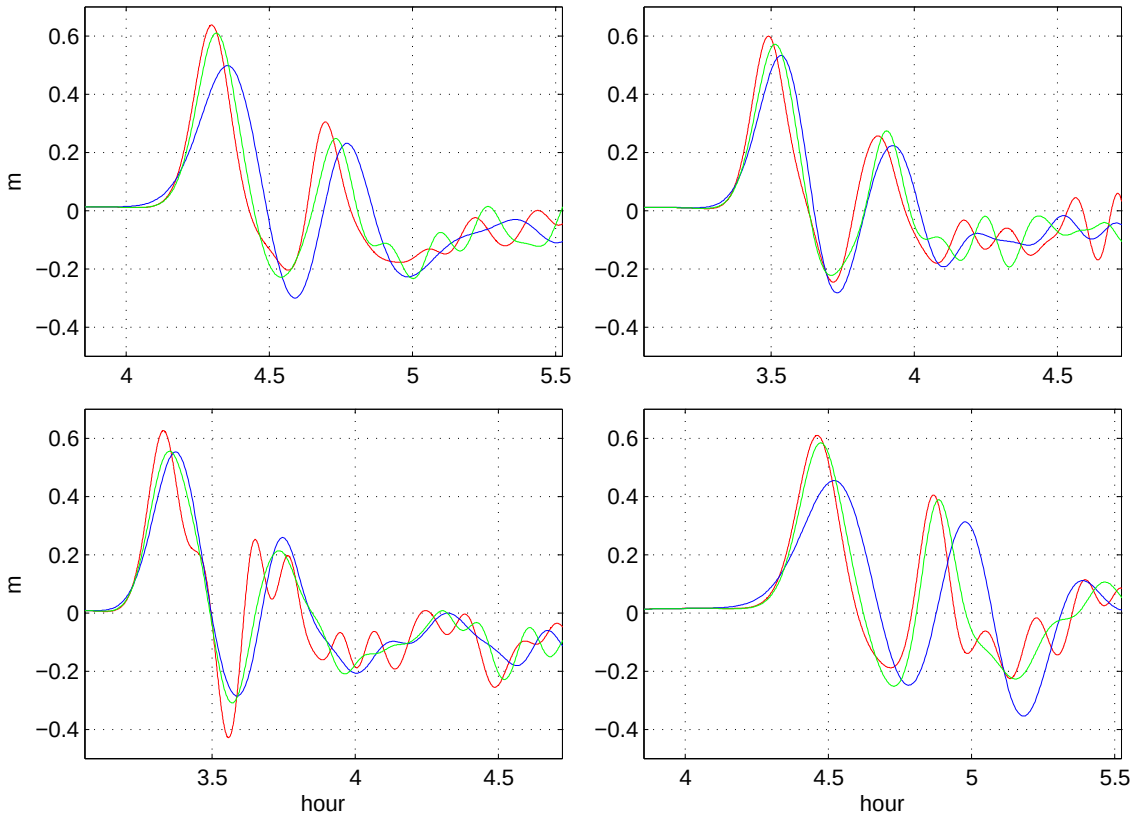

Figure 7: B-boundary timeseries at nodes 200, 450, 700, and 900 from larger A grid at 30 s (red) and smaller Agrids at 60 s (blue), and 30 s (green) resolution. Grid-test event.

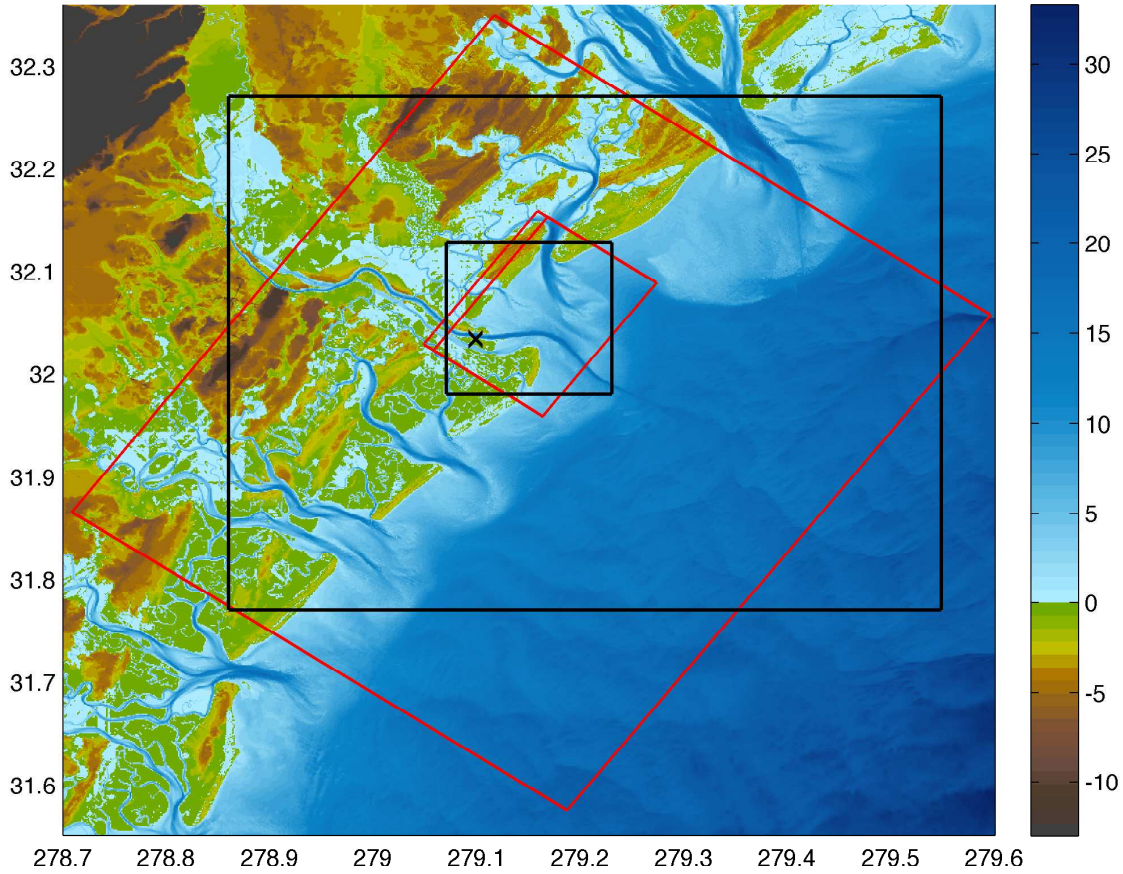

Figure 8: B and C grids for v.4 (red) and v.2 (black) cut from Savannah DEM. Reference and optimized C grids for v.4 coincide on 3 sides, but the former extends further inland. X-axis: longitude, degree East, Y-axis - latitude, degree North. Cross shows the tide gage location. Colorscale: meters.

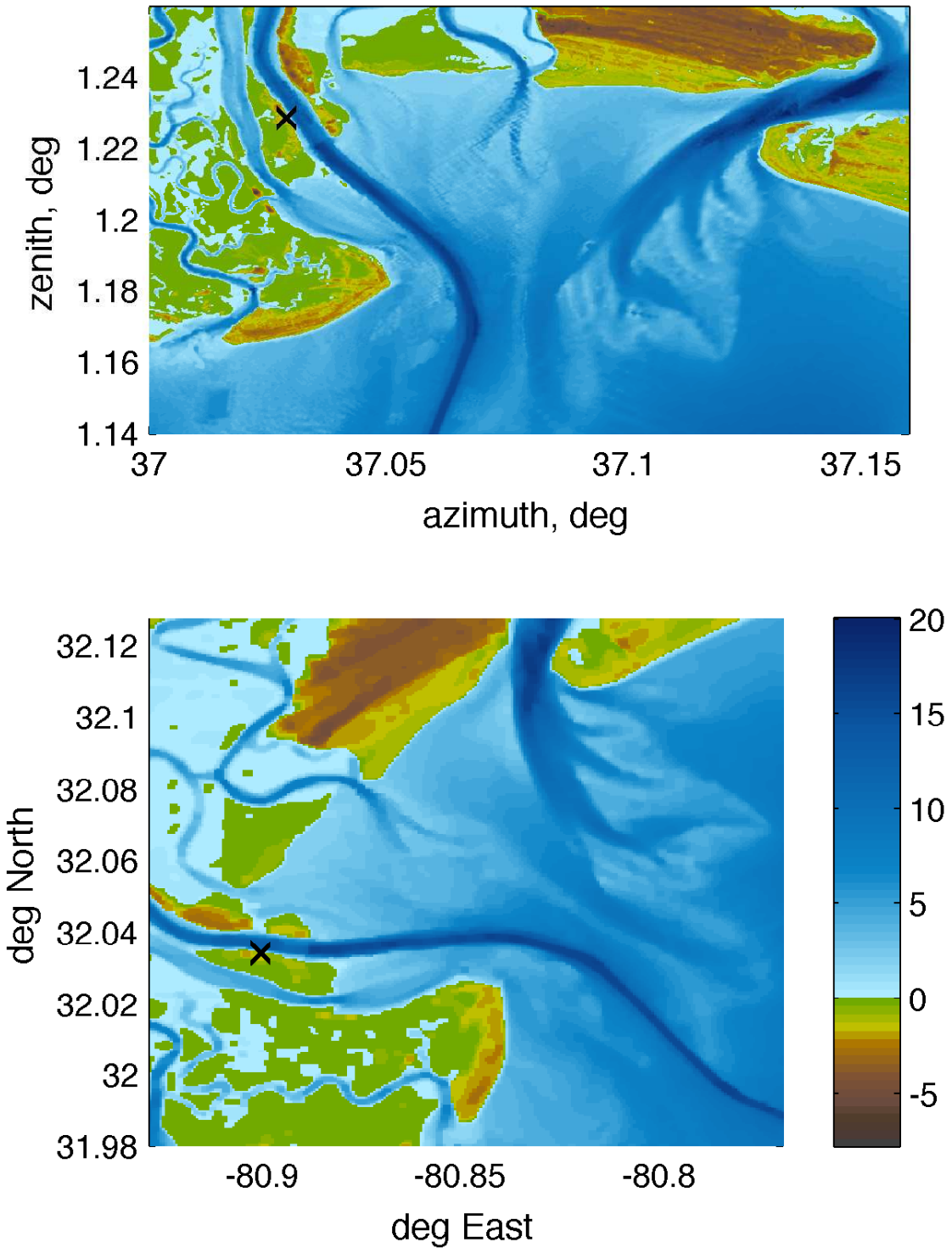

Figure 9: Reference v.4 (top) and optimized v_2^2 (bottom) C grids. Cross shows the tide gage location in each grid. Colorscale: meters.

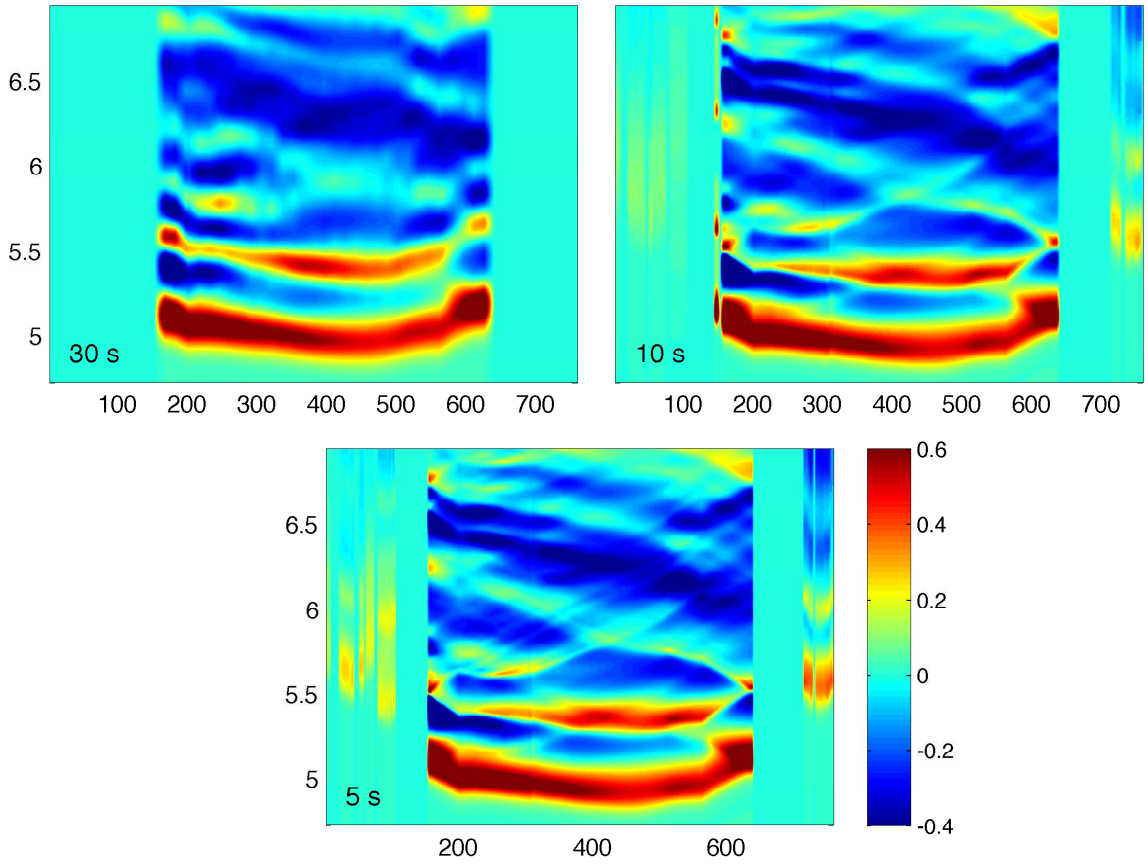

Figure 10: Boundary input into optimized C grid from the optimized A (30 s, no topography) and B grids at 10 s and 5 s resolution containing topography. Y-axis: hour, X-axis: node along the C-boundary, colorscale: meters. Grid-test event.

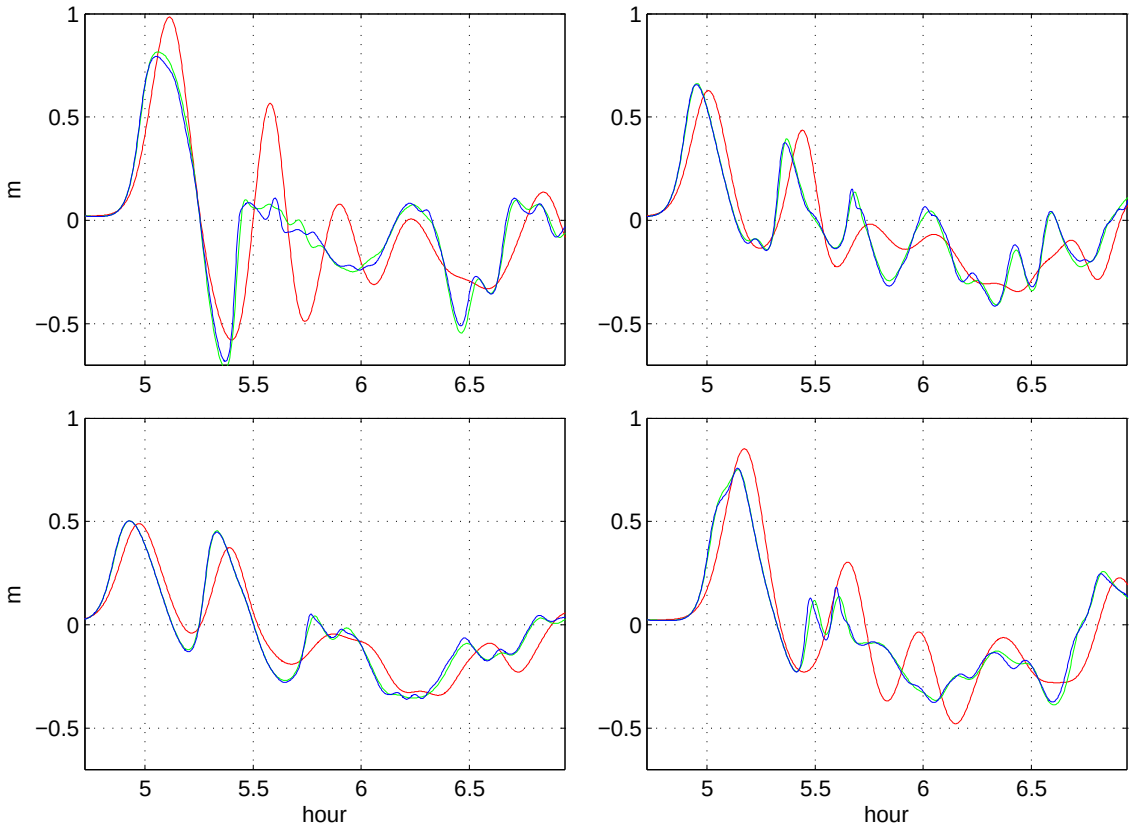

Figure 11: C-boundary timeseries at nodes 180, 330, 480, and 610 (counting from the grid's West corner along the ocean-side boundary) computed in A grid at 30 s (red), and refined with B grid at 10 s (green) and 5 s (blue) resolution. Grid-test event.

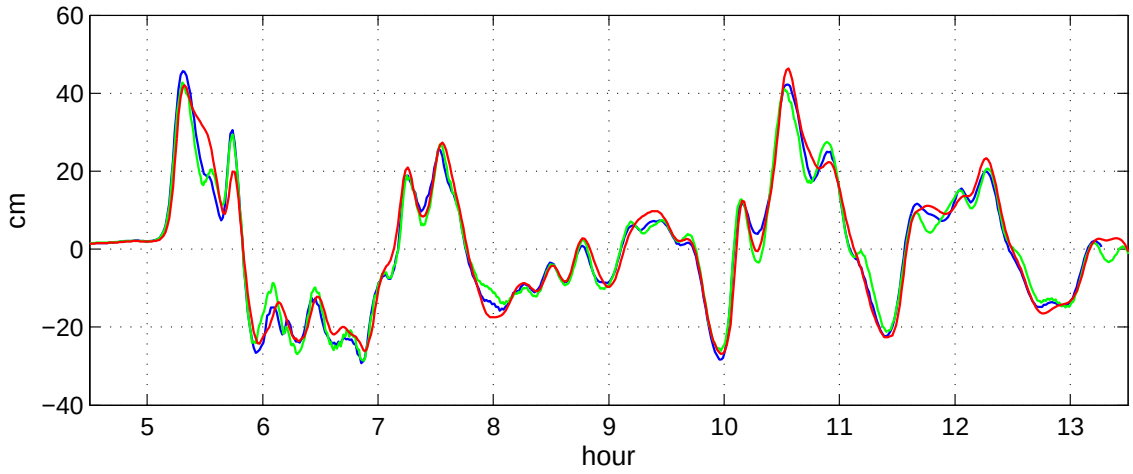

Figure 12: Time history at the gage computed in B-grid (red), optimized C grid at 2 s (green) and reference C grid at 0.7 s (blue) resolution. Grid-test event.

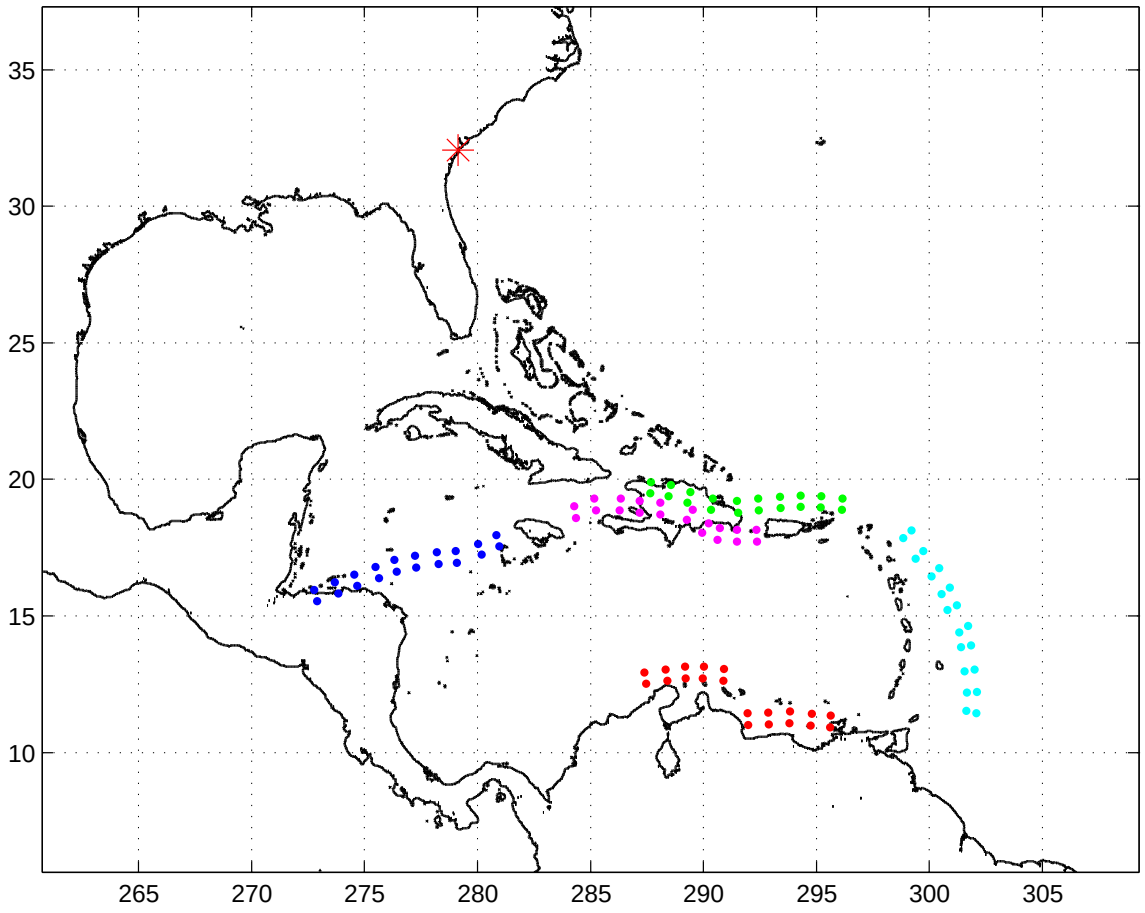

Figure 13: Synthetic mega event origins in the Caribbean: dots represent unit sources for Mega 1 event (red), Mega 2 (cyan), Mega 3 (green), Mega 4 (blue), Mega 5 (magenta). Red star - Savannah model area.

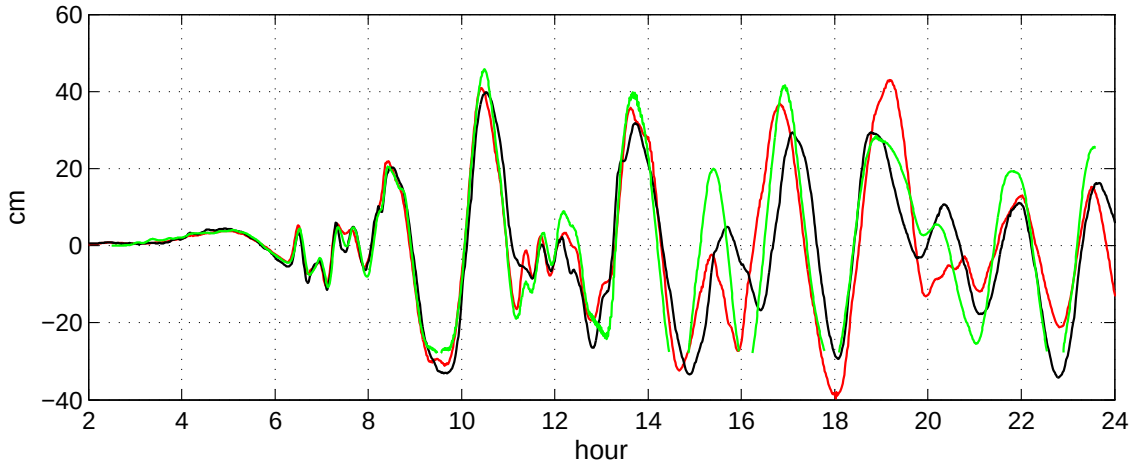

Figure 14: Mega 1. Time history at the gage location according to Forecast Model v.2 (black), Forecast Model v.4 (green), and Reference Model v.4 (red).

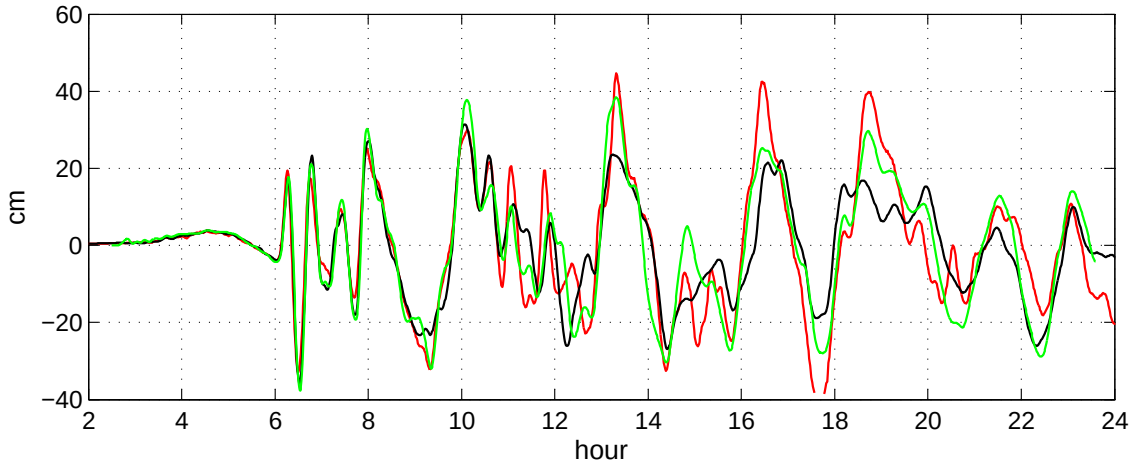

Figure 15: Mega 1. Time history at the second observation point according to Forecast Model v.2 (black), Forecast Model v.4 (green), and Reference Model v.4 (red)

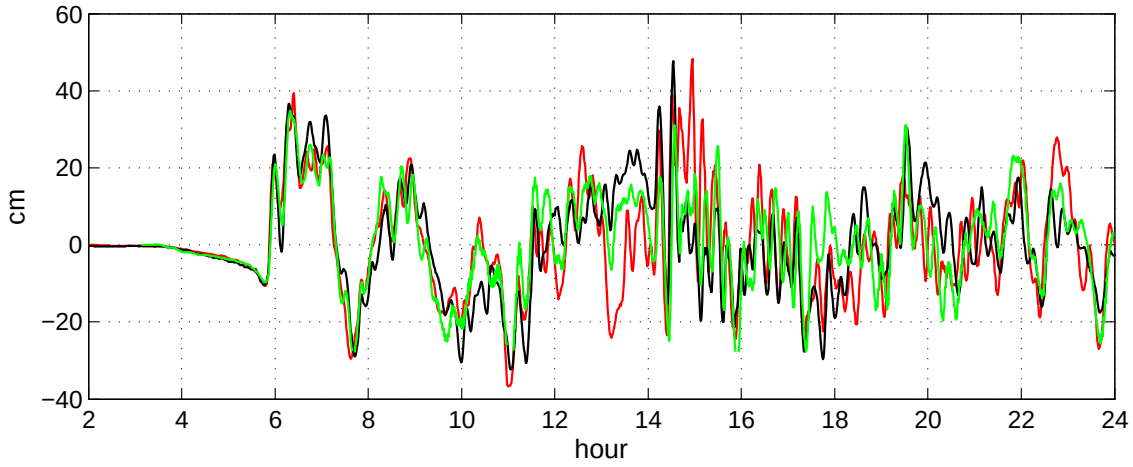

Figure 16: Mega 2. Same as above, at the gage location.

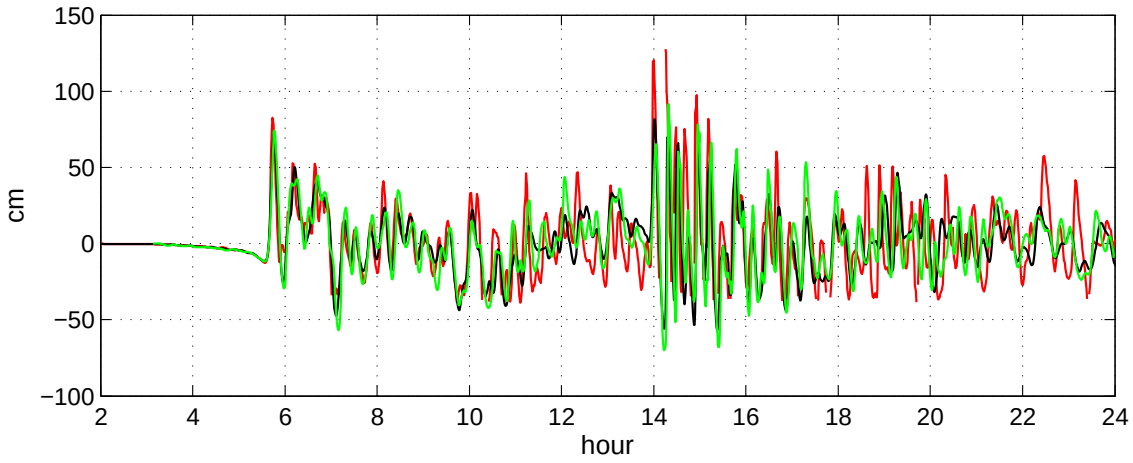

Figure 17: Mega 2. Same as above, at the second observation point.

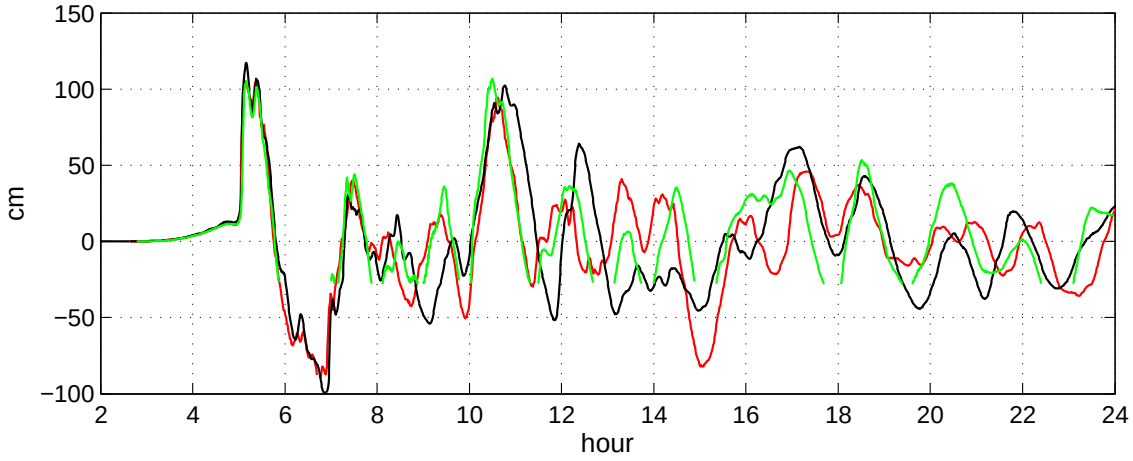

Figure 18: Mega 3. Same as above, at the gage location.

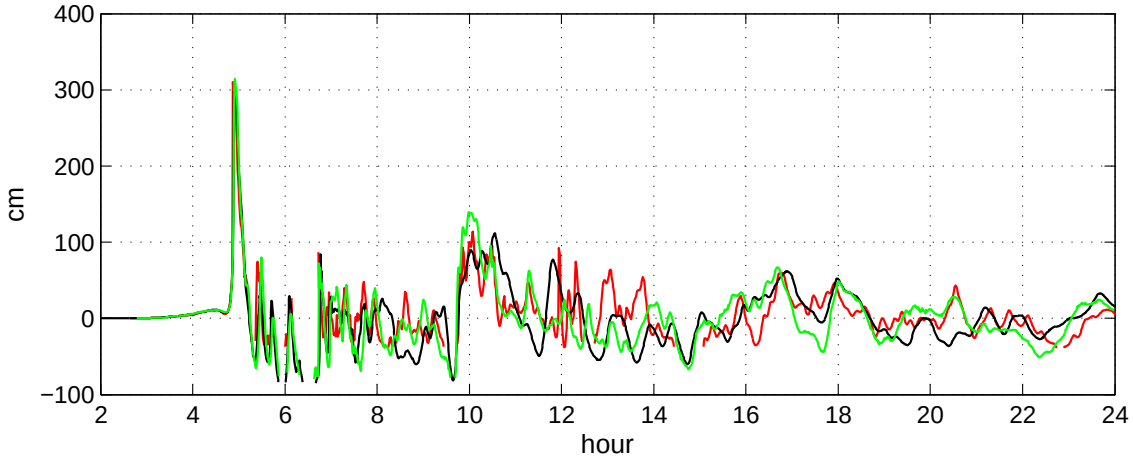

Figure 19: Mega 3. Same as above, at the second observation point.

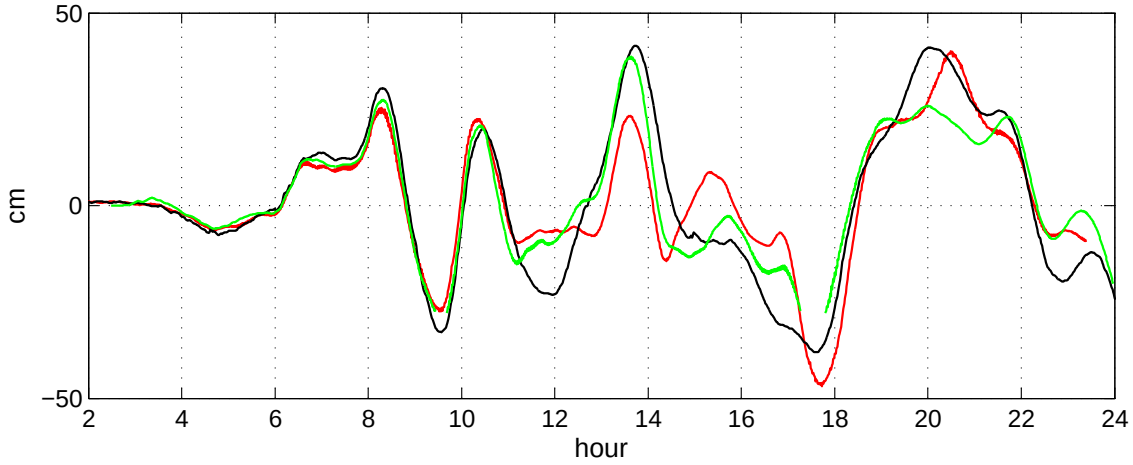

Figure 20: Mega 4. Same as above, at the gage location.

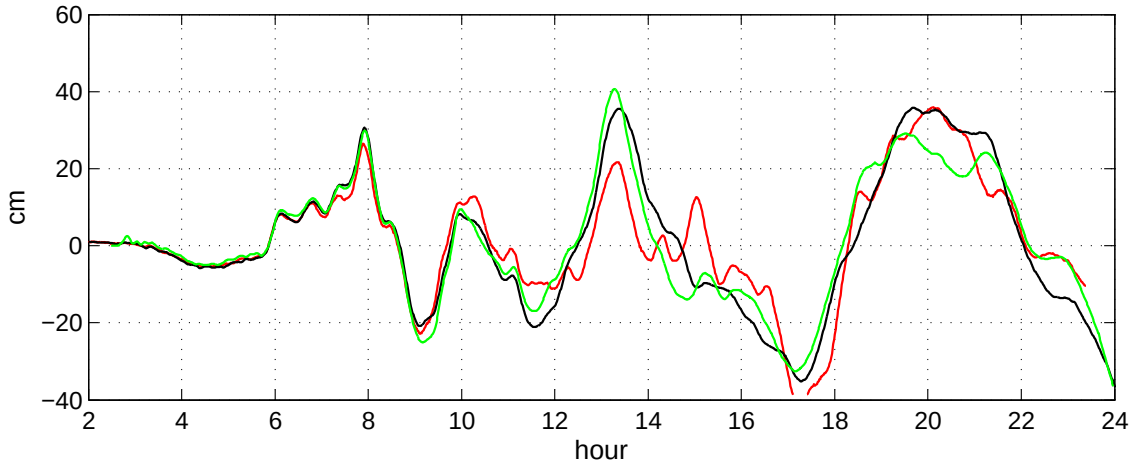

Figure 21: Mega 4. Same as above, at the second observation point.

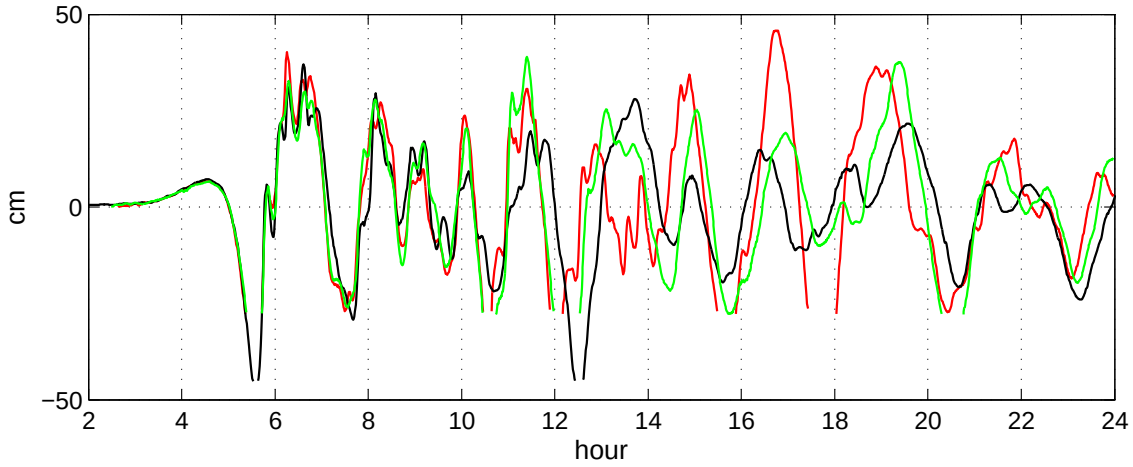

Figure 22: Mega 5. Same as above, at the gage location.

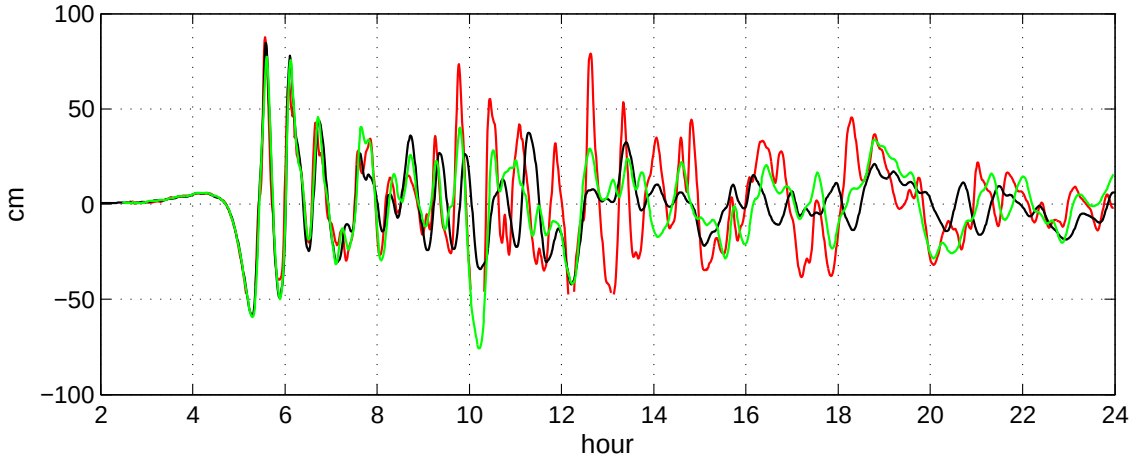

Figure 23: Mega 5. Same as above, at the second observation point.

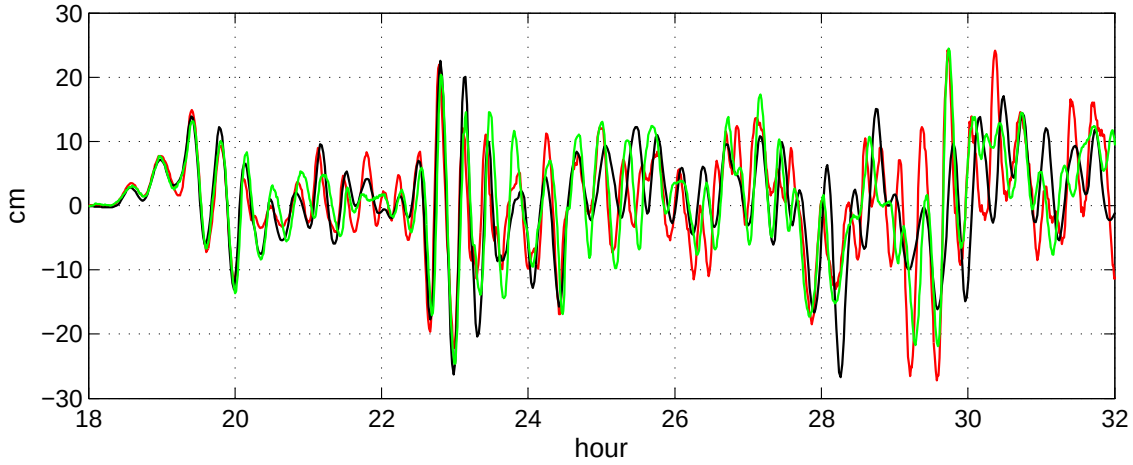

Figure 24: Mega 6. Same as above, at the gage location.

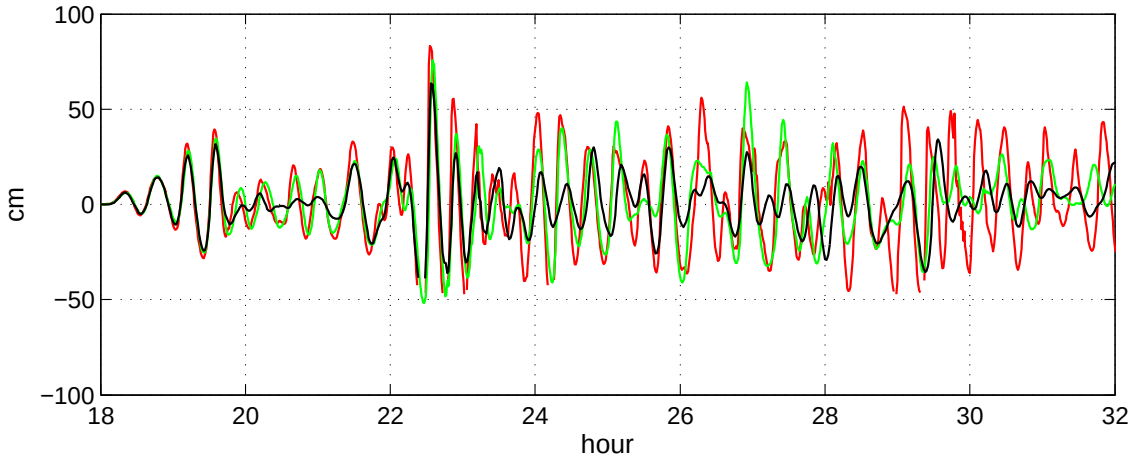

Figure 25: Mega 6. Same as above, at the second observation point.

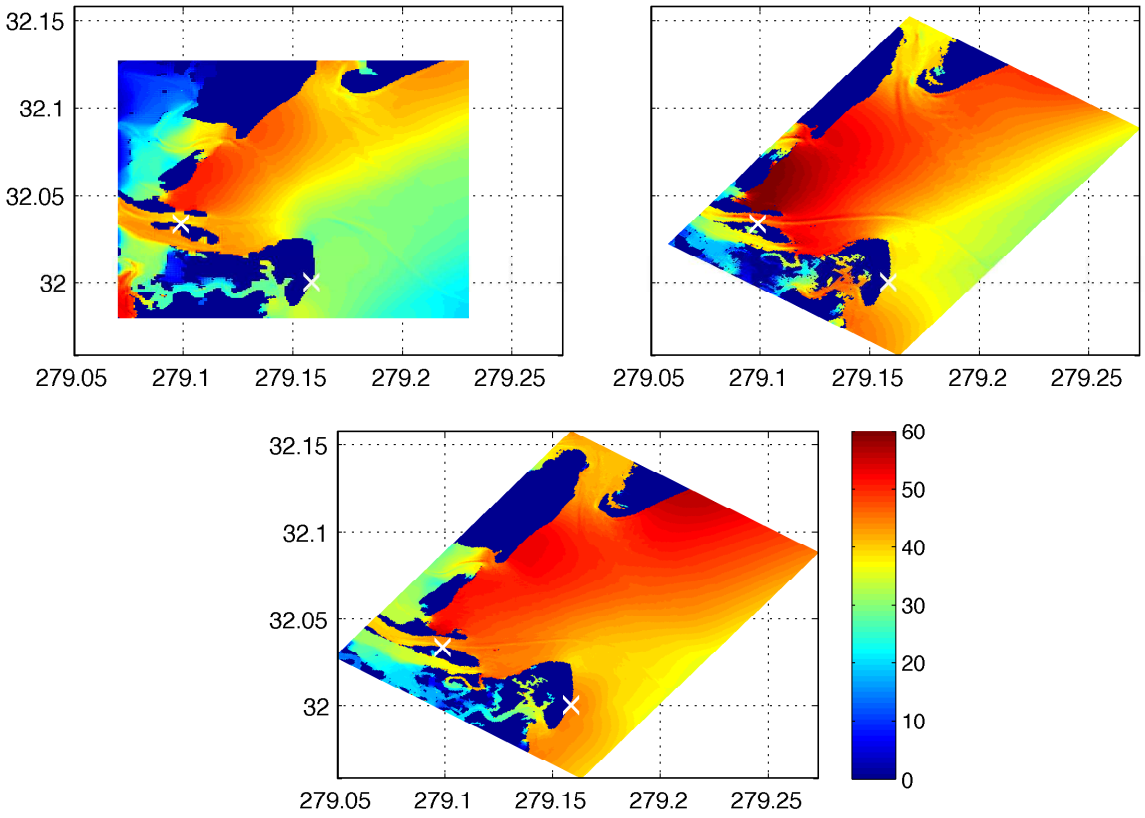

Figure 26: Mega 1. Maximum wave elevation within C grid, according to Forecast Model v.2 (top left), Forecast Model v.4 (top right) and Reference model v.4 (bottom). X-axis: longitude, degree East, Y-axis - latitude, degree North. Colorscale: cm. White crosses: observation points.

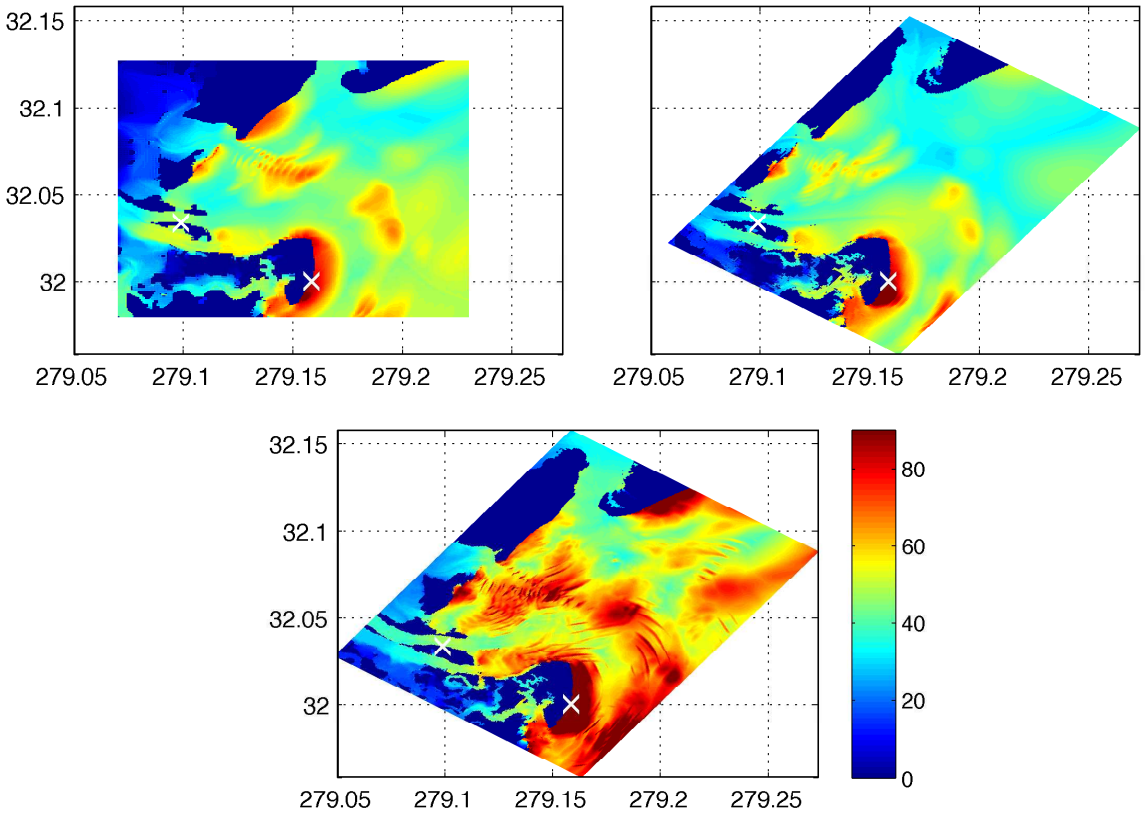

Figure 27: Same as above for Mega 2 event.

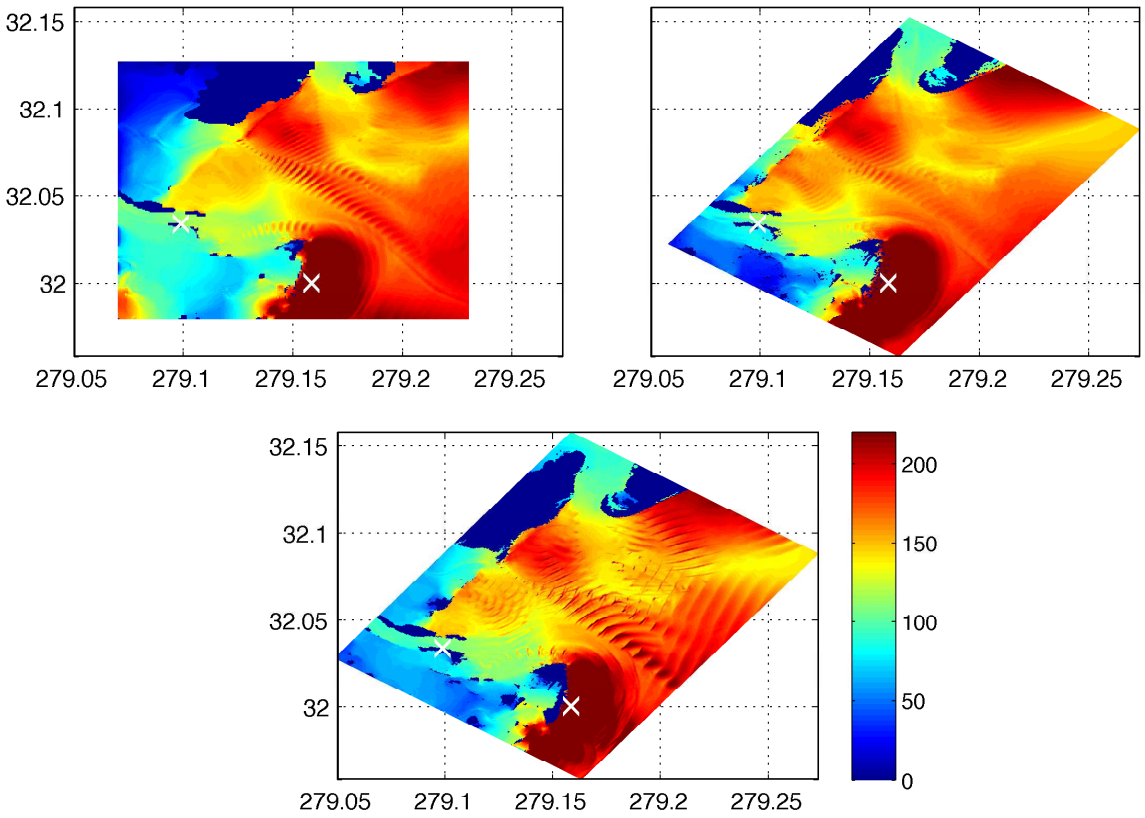

Figure 28: Same as above for Mega 3 event.

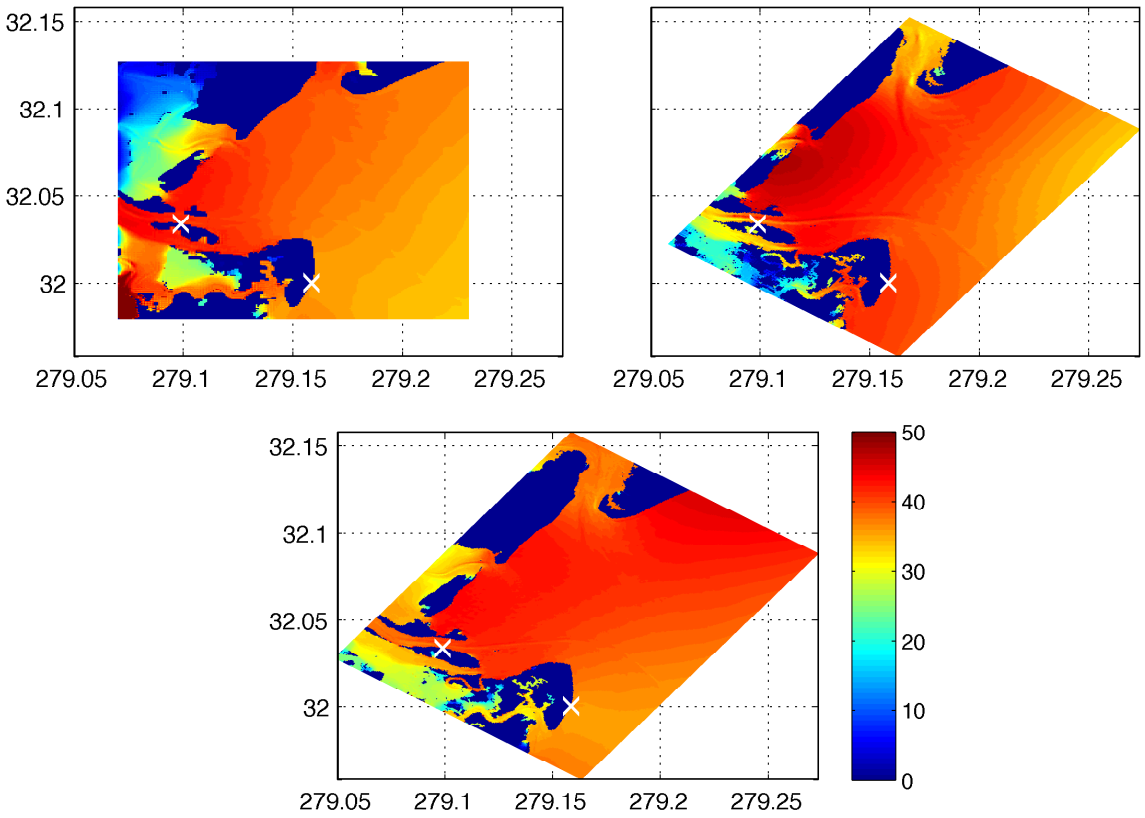

Figure 29: Same as above for Mega 4 event.

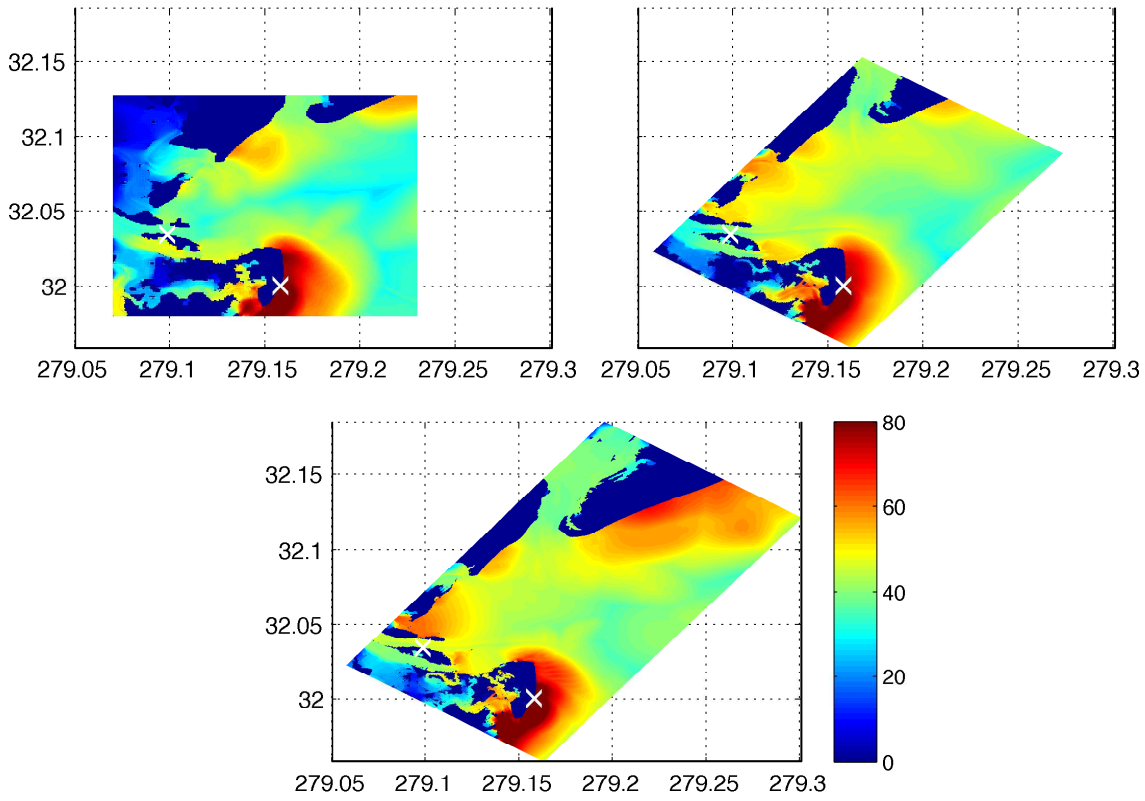

Figure 30: Same as above for Mega 5 event.

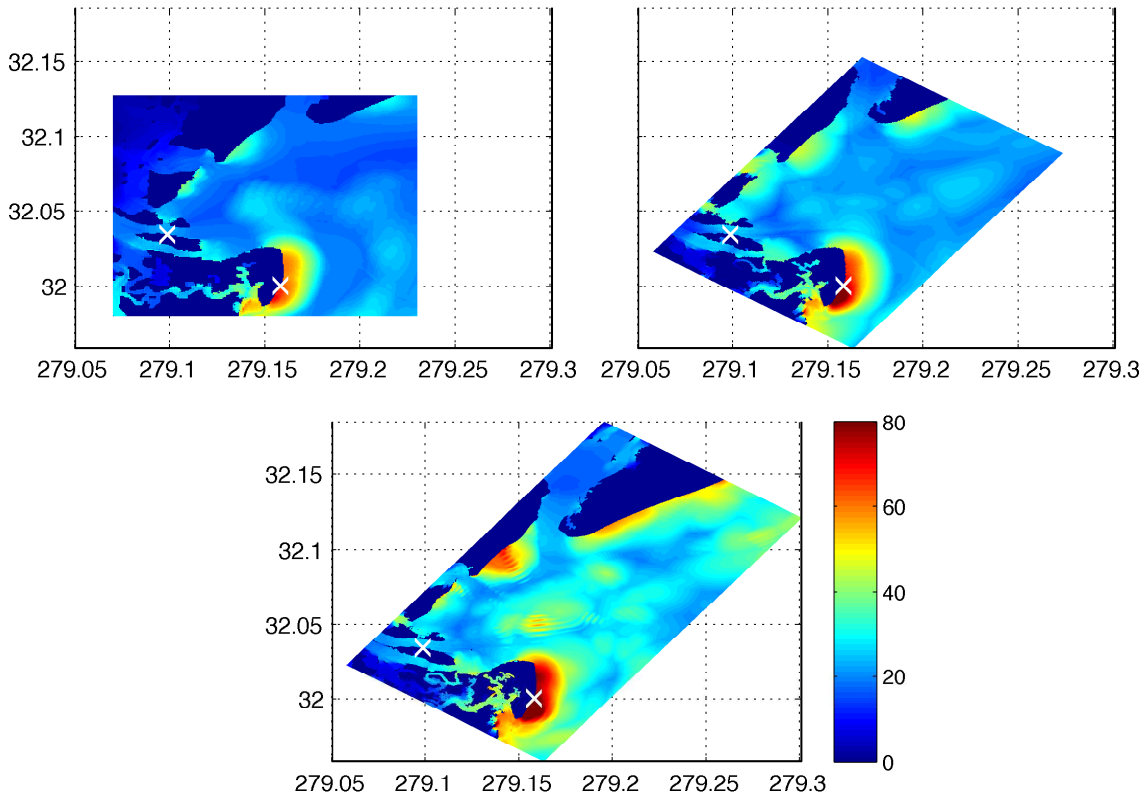

Figure 31: Same as above for Mega 6 event.

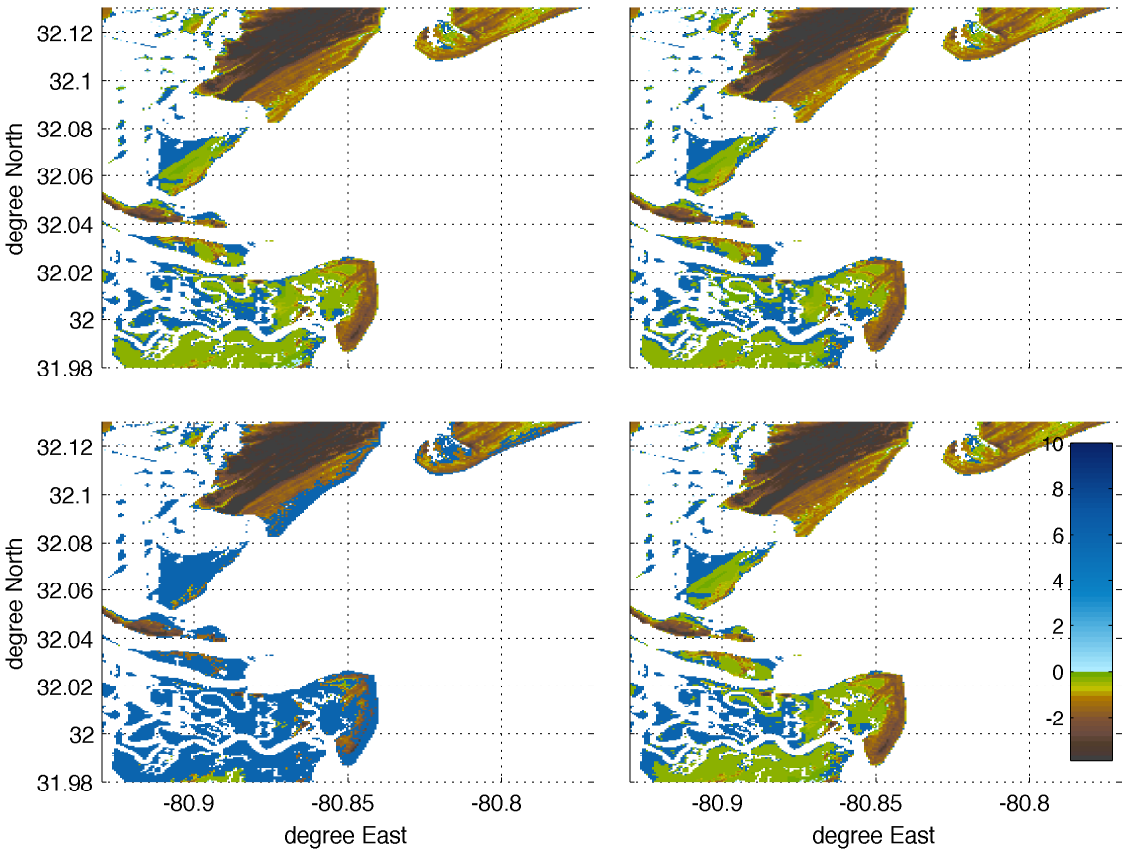

Figure 32: Area inundated by mega tsunamis (event Mega 1 (top left), Mega 2 (top right), Mega 3 (bottom left), and Mega 4 (bottom right)), according to the operational Forecast Model, MOST v.2. Only originally dry land is shown, with inundated area shown in blue. Colorscale - meters (does not apply to the inundated area).

B Propagation Database: Atlantic Ocean Unit Sources

Propagation source details reflect the database as of January 2010. There may have been updates in the earthquake source parameters after this date.

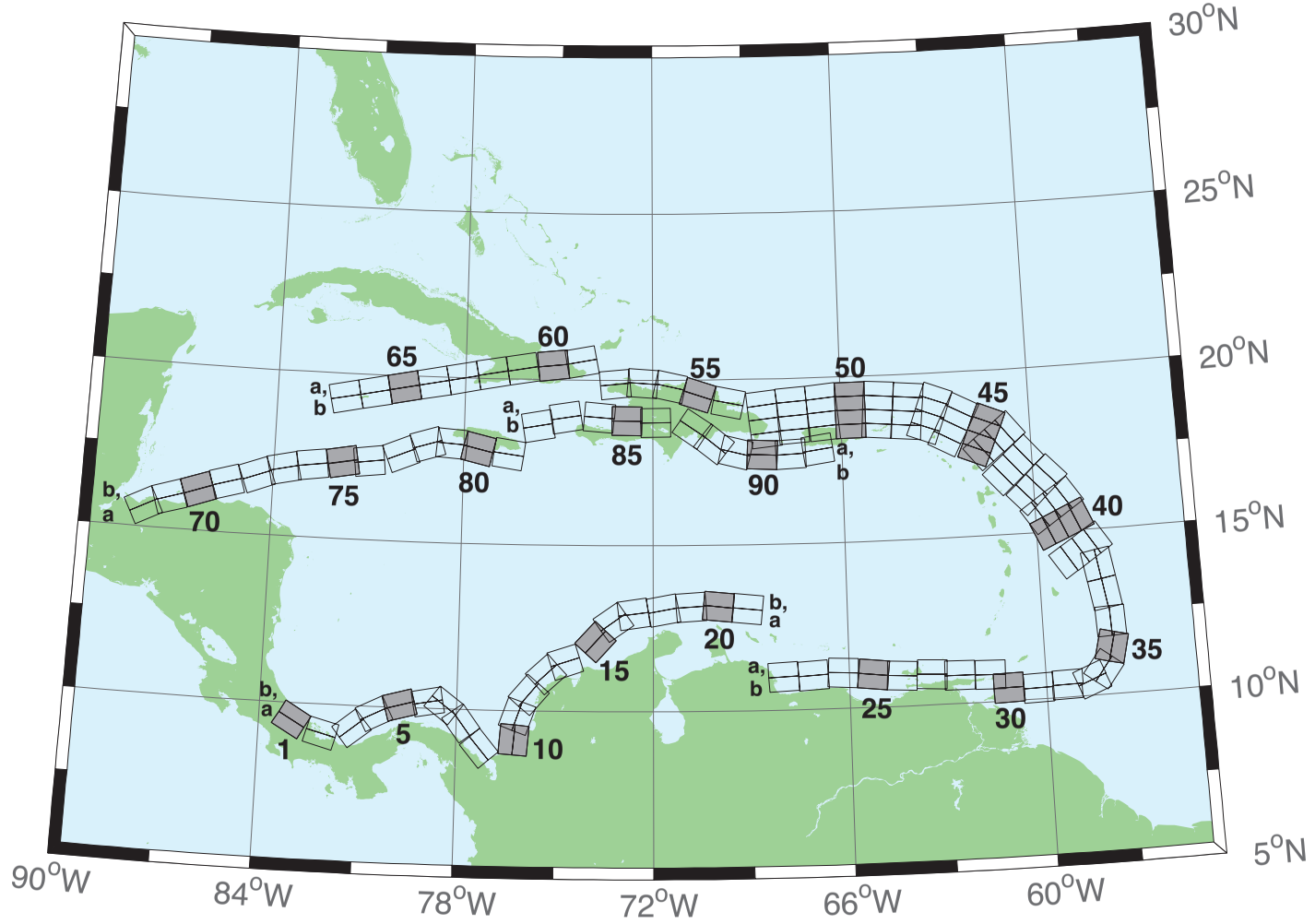

Figure 33: Atlantic Source Zone unit sources.

Table 5: Earthquake parameters for Atlantic Source Zone unit sources.

Segment	Description	Longitude(°E)	Latitude(°N)	Strike(°)	Dip(°)	Depth (km)
atsz–1a	Atlantic Source Zone	-83.2020	9.1449	120	27.5	28.09
atsz–1b	Atlantic Source Zone	-83.0000	9.4899	120	27.5	5
atsz–2a	Atlantic Source Zone	-82.1932	8.7408	105.1	27.5	28.09
atsz–2b	Atlantic Source Zone	-82.0880	9.1254	105.1	27.5	5
atsz–3a	Atlantic Source Zone	-80.9172	9.0103	51.31	30	30
atsz–3b	Atlantic Source Zone	-81.1636	9.3139	51.31	30	5
atsz–4a	Atlantic Source Zone	-80.3265	9.4308	63.49	30	30
atsz–4b	Atlantic Source Zone	-80.5027	9.7789	63.49	30	5
atsz–5a	Atlantic Source Zone	-79.6247	9.6961	74.44	30	30
atsz–5b	Atlantic Source Zone	-79.7307	10.0708	74.44	30	5
atsz–6a	Atlantic Source Zone	-78.8069	9.8083	79.71	30	30
atsz–6b	Atlantic Source Zone	-78.8775	10.1910	79.71	30	5
atsz–7a	Atlantic Source Zone	-78.6237	9.7963	127.2	30	30
atsz–7b	Atlantic Source Zone	-78.3845	10.1059	127.2	30	5
atsz–8a	Atlantic Source Zone	-78.1693	9.3544	143.8	30	30
atsz–8b	Atlantic Source Zone	-77.8511	9.5844	143.8	30	5
atsz–9a	Atlantic Source Zone	-77.5913	8.5989	139.9	30	30
atsz–9b	Atlantic Source Zone	-77.2900	8.8493	139.9	30	5
atsz–10a	Atlantic Source Zone	-75.8109	9.0881	4.67	17	19.62
atsz–10b	Atlantic Source Zone	-76.2445	9.1231	4.67	17	5
atsz–11a	Atlantic Source Zone	-75.7406	9.6929	19.67	17	19.62
atsz–11b	Atlantic Source Zone	-76.1511	9.8375	19.67	17	5
atsz–12a	Atlantic Source Zone	-75.4763	10.2042	40.4	17	19.62
atsz–12b	Atlantic Source Zone	-75.8089	10.4826	40.4	17	5
atsz–13a	Atlantic Source Zone	-74.9914	10.7914	47.17	17	19.62
atsz–13b	Atlantic Source Zone	-75.2890	11.1064	47.17	17	5
atsz–14a	Atlantic Source Zone	-74.5666	11.0708	71.68	17	19.62
atsz–14b	Atlantic Source Zone	-74.7043	11.4786	71.68	17	5
atsz–15a	Atlantic Source Zone	-73.4576	11.8012	42.69	17	19.62
atsz–15b	Atlantic Source Zone	-73.7805	12.0924	42.69	17	5
atsz–16a	Atlantic Source Zone	-72.9788	12.3365	54.75	17	19.62
atsz–16b	Atlantic Source Zone	-73.2329	12.6873	54.75	17	5
atsz–17a	Atlantic Source Zone	-72.5454	12.5061	81.96	17	19.62
atsz–17b	Atlantic Source Zone	-72.6071	12.9314	81.96	17	5
atsz–18a	Atlantic Source Zone	-71.6045	12.6174	79.63	17	19.62
atsz–18b	Atlantic Source Zone	-71.6839	13.0399	79.63	17	5
atsz–19a	Atlantic Source Zone	-70.7970	12.7078	86.32	17	19.62
atsz–19b	Atlantic Source Zone	-70.8253	13.1364	86.32	17	5
atsz–20a	Atlantic Source Zone	-70.0246	12.7185	95.94	17	19.62
atsz–20b	Atlantic Source Zone	-69.9789	13.1457	95.94	17	5
atsz–21a	Atlantic Source Zone	-69.1244	12.6320	95.94	17	19.62
atsz–21b	Atlantic Source Zone	-69.0788	13.0592	95.94	17	5
atsz–22a	Atlantic Source Zone	-68.0338	11.4286	266.9	15	17.94
atsz–22b	Atlantic Source Zone	-68.0102	10.9954	266.9	15	5
atsz–23a	Atlantic Source Zone	-67.1246	11.4487	266.9	15	17.94
atsz–23b	Atlantic Source Zone	-67.1010	11.0155	266.9	15	5
atsz–24a	Atlantic Source Zone	-66.1656	11.5055	273.3	15	17.94
atsz–24b	Atlantic Source Zone	-66.1911	11.0724	273.3	15	5
atsz–25a	Atlantic Source Zone	-65.2126	11.4246	276.4	15	17.94
atsz–25b	Atlantic Source Zone	-65.2616	10.9934	276.4	15	5
atsz–26a	Atlantic Source Zone	-64.3641	11.3516	272.9	15	17.94
atsz–26b	Atlantic Source Zone	-64.3862	10.9183	272.9	15	5
atsz–27a	Atlantic Source Zone	-63.4472	11.3516	272.9	15	17.94
atsz–27b	Atlantic Source Zone	-63.4698	10.9183	272.9	15	5
atsz–28a	Atlantic Source Zone	-62.6104	11.2831	271.1	15	17.94
atsz–28b	Atlantic Source Zone	-62.6189	10.8493	271.1	15	5
atsz–29a	Atlantic Source Zone	-61.6826	11.2518	271.6	15	17.94
atsz–29b	Atlantic Source Zone	-61.6947	10.8181	271.6	15	5
atsz–30a	Atlantic Source Zone	-61.1569	10.8303	269	15	17.94
atsz–30b	Atlantic Source Zone	-61.1493	10.3965	269	15	5
atsz–31a	Atlantic Source Zone	-60.2529	10.7739	269	15	17.94
atsz–31b	Atlantic Source Zone	-60.2453	10.3401	269	15	5
atsz–32a	Atlantic Source Zone	-59.3510	10.8123	269	15	17.94
atsz–32b	Atlantic Source Zone	-59.3734	10.3785	269	15	5
atsz–33a	Atlantic Source Zone	-58.7592	10.8785	248.6	15	17.94

Continued on next page

Table 5 – continued from previous page

Segment	Description	Longitude(°E)	Latitude(°N)	Strike(°)	Dip(°)	Depth (km)
atsz–33b	Atlantic Source Zone	-58.5984	10.4745	248.6	15	5
atsz–34a	Atlantic Source Zone	-58.5699	11.0330	217.2	15	17.94
atsz–34b	Atlantic Source Zone	-58.2179	10.7710	217.2	15	5
atsz–35a	Atlantic Source Zone	-58.3549	11.5300	193.7	15	17.94
atsz–35b	Atlantic Source Zone	-57.9248	11.4274	193.7	15	5
atsz–36a	Atlantic Source Zone	-58.3432	12.1858	177.7	15	17.94
atsz–36b	Atlantic Source Zone	-57.8997	12.2036	177.7	15	5
atsz–37a	Atlantic Source Zone	-58.4490	12.9725	170.7	15	17.94
atsz–37b	Atlantic Source Zone	-58.0095	13.0424	170.7	15	5
atsz–38a	Atlantic Source Zone	-58.6079	13.8503	170.2	15	17.94
atsz–38b	Atlantic Source Zone	-58.1674	13.9240	170.2	15	5
atsz–39a	Atlantic Source Zone	-58.6667	14.3915	146.8	15	17.94
atsz–39b	Atlantic Source Zone	-58.2913	14.6287	146.8	15	5
atsz–39y	Atlantic Source Zone	-59.4168	13.9171	146.8	15	43.82
atsz–39z	Atlantic Source Zone	-59.0415	14.1543	146.8	15	30.88
atsz–40a	Atlantic Source Zone	-59.1899	15.2143	156.2	15	17.94
atsz–40b	Atlantic Source Zone	-58.7781	15.3892	156.2	15	5
atsz–40y	Atlantic Source Zone	-60.0131	14.8646	156.2	15	43.82
atsz–40z	Atlantic Source Zone	-59.6012	15.0395	156.2	15	30.88
atsz–41a	Atlantic Source Zone	-59.4723	15.7987	146.3	15	17.94
atsz–41b	Atlantic Source Zone	-59.0966	16.0392	146.3	15	5
atsz–41y	Atlantic Source Zone	-60.2229	15.3177	146.3	15	43.82
atsz–41z	Atlantic Source Zone	-59.8473	15.5582	146.3	15	30.88
atsz–42a	Atlantic Source Zone	-59.9029	16.4535	137	15	17.94
atsz–42b	Atlantic Source Zone	-59.5716	16.7494	137	15	5
atsz–42y	Atlantic Source Zone	-60.5645	15.8616	137	15	43.82
atsz–42z	Atlantic Source Zone	-60.2334	16.1575	137	15	30.88
atsz–43a	Atlantic Source Zone	-60.5996	17.0903	138.7	15	17.94
atsz–43b	Atlantic Source Zone	-60.2580	17.3766	138.7	15	5
atsz–43y	Atlantic Source Zone	-61.2818	16.5177	138.7	15	43.82
atsz–43z	Atlantic Source Zone	-60.9404	16.8040	138.7	15	30.88
atsz–44a	Atlantic Source Zone	-61.1559	17.8560	141.1	15	17.94
atsz–44b	Atlantic Source Zone	-60.8008	18.1286	141.1	15	5
atsz–44y	Atlantic Source Zone	-61.8651	17.3108	141.1	15	43.82
atsz–44z	Atlantic Source Zone	-61.5102	17.5834	141.1	15	30.88
atsz–45a	Atlantic Source Zone	-61.5491	18.0566	112.8	15	17.94
atsz–45b	Atlantic Source Zone	-61.3716	18.4564	112.8	15	5
atsz–45y	Atlantic Source Zone	-61.9037	17.2569	112.8	15	43.82
atsz–45z	Atlantic Source Zone	-61.7260	17.6567	112.8	15	30.88
atsz–46a	Atlantic Source Zone	-62.4217	18.4149	117.9	15	17.94
atsz–46b	Atlantic Source Zone	-62.2075	18.7985	117.9	15	5
atsz–46y	Atlantic Source Zone	-62.8493	17.6477	117.9	15	43.82
atsz–46z	Atlantic Source Zone	-62.6352	18.0313	117.9	15	30.88
atsz–47a	Atlantic Source Zone	-63.1649	18.7844	110.5	20	22.1
atsz–47b	Atlantic Source Zone	-63.0087	19.1798	110.5	20	5
atsz–47y	Atlantic Source Zone	-63.4770	17.9936	110.5	20	56.3
atsz–47z	Atlantic Source Zone	-63.3205	18.3890	110.5	20	39.2
atsz–48a	Atlantic Source Zone	-63.8800	18.8870	95.37	20	22.1
atsz–48b	Atlantic Source Zone	-63.8382	19.3072	95.37	20	5
atsz–48y	Atlantic Source Zone	-63.9643	18.0465	95.37	20	56.3
atsz–48z	Atlantic Source Zone	-63.9216	18.4667	95.37	20	39.2
atsz–49a	Atlantic Source Zone	-64.8153	18.9650	94.34	20	22.1
atsz–49b	Atlantic Source Zone	-64.7814	19.3859	94.34	20	5
atsz–49y	Atlantic Source Zone	-64.8840	18.1233	94.34	20	56.3
atsz–49z	Atlantic Source Zone	-64.8492	18.5442	94.34	20	39.2
atsz–50a	Atlantic Source Zone	-65.6921	18.9848	89.59	20	22.1
atsz–50b	Atlantic Source Zone	-65.6953	19.4069	89.59	20	5
atsz–50y	Atlantic Source Zone	-65.6874	18.1407	89.59	20	56.3
atsz–50z	Atlantic Source Zone	-65.6887	18.5628	89.59	20	39.2
atsz–51a	Atlantic Source Zone	-66.5742	18.9484	84.98	20	22.1
atsz–51b	Atlantic Source Zone	-66.6133	19.3688	84.98	20	5
atsz–51y	Atlantic Source Zone	-66.4977	18.1076	84.98	20	56.3
atsz–51z	Atlantic Source Zone	-66.5353	18.5280	84.98	20	39.2
atsz–52a	Atlantic Source Zone	-67.5412	18.8738	85.87	20	22.1
atsz–52b	Atlantic Source Zone	-67.5734	19.2948	85.87	20	5
atsz–52y	Atlantic Source Zone	-67.4781	18.0319	85.87	20	56.3

Continued on next page

Table 5 – continued from previous page

Segment	Description	Longitude(°E)	Latitude(°N)	Strike(°)	Dip(°)	Depth (km)
atsz–52z	Atlantic Source Zone	-67.5090	18.4529	85.87	20	39.2
atsz–53a	Atlantic Source Zone	-68.4547	18.7853	83.64	20	22.1
atsz–53b	Atlantic Source Zone	-68.5042	19.2048	83.64	20	5
atsz–53y	Atlantic Source Zone	-68.3575	17.9463	83.64	20	56.3
atsz–53z	Atlantic Source Zone	-68.4055	18.3658	83.64	20	39.2
atsz–54a	Atlantic Source Zone	-69.6740	18.8841	101.5	20	22.1
atsz–54b	Atlantic Source Zone	-69.5846	19.2976	101.5	20	5
atsz–55a	Atlantic Source Zone	-70.7045	19.1376	108.2	20	22.1
atsz–55b	Atlantic Source Zone	-70.5647	19.5386	108.2	20	5
atsz–56a	Atlantic Source Zone	-71.5368	19.3853	102.6	20	22.1
atsz–56b	Atlantic Source Zone	-71.4386	19.7971	102.6	20	5
atsz–57a	Atlantic Source Zone	-72.3535	19.4838	94.2	20	22.1
atsz–57b	Atlantic Source Zone	-72.3206	19.9047	94.2	20	5
atsz–58a	Atlantic Source Zone	-73.1580	19.4498	84.34	20	22.1
atsz–58b	Atlantic Source Zone	-73.2022	19.8698	84.34	20	5
atsz–59a	Atlantic Source Zone	-74.3567	20.9620	259.7	20	22.1
atsz–59b	Atlantic Source Zone	-74.2764	20.5467	259.7	20	5
atsz–60a	Atlantic Source Zone	-75.2386	20.8622	264.2	15	17.94
atsz–60b	Atlantic Source Zone	-75.1917	20.4306	264.2	15	5
atsz–61a	Atlantic Source Zone	-76.2383	20.7425	260.7	15	17.94
atsz–61b	Atlantic Source Zone	-76.1635	20.3144	260.7	15	5
atsz–62a	Atlantic Source Zone	-77.2021	20.5910	259.9	15	17.94
atsz–62b	Atlantic Source Zone	-77.1214	20.1638	259.9	15	5
atsz–63a	Atlantic Source Zone	-78.1540	20.4189	259	15	17.94
atsz–63b	Atlantic Source Zone	-78.0661	19.9930	259	15	5
atsz–64a	Atlantic Source Zone	-79.0959	20.2498	259.2	15	17.94
atsz–64b	Atlantic Source Zone	-79.0098	19.8236	259.2	15	5
atsz–65a	Atlantic Source Zone	-80.0393	20.0773	258.9	15	17.94
atsz–65b	Atlantic Source Zone	-79.9502	19.6516	258.9	15	5
atsz–66a	Atlantic Source Zone	-80.9675	19.8993	258.6	15	17.94
atsz–66b	Atlantic Source Zone	-80.8766	19.4740	258.6	15	5
atsz–67a	Atlantic Source Zone	-81.9065	19.7214	258.5	15	17.94
atsz–67b	Atlantic Source Zone	-81.8149	19.2962	258.5	15	5
atsz–68a	Atlantic Source Zone	-87.8003	15.2509	62.69	15	17.94
atsz–68b	Atlantic Source Zone	-88.0070	15.6364	62.69	15	5
atsz–69a	Atlantic Source Zone	-87.0824	15.5331	72.73	15	17.94
atsz–69b	Atlantic Source Zone	-87.2163	15.9474	72.73	15	5
atsz–70a	Atlantic Source Zone	-86.1622	15.8274	70.64	15	17.94
atsz–70b	Atlantic Source Zone	-86.3120	16.2367	70.64	15	5
atsz–71a	Atlantic Source Zone	-85.3117	16.1052	73.7	15	17.94
atsz–71b	Atlantic Source Zone	-85.4387	16.5216	73.7	15	5
atsz–72a	Atlantic Source Zone	-84.3470	16.3820	69.66	15	17.94
atsz–72b	Atlantic Source Zone	-84.5045	16.7888	69.66	15	5
atsz–73a	Atlantic Source Zone	-83.5657	16.6196	77.36	15	17.94
atsz–73b	Atlantic Source Zone	-83.6650	17.0429	77.36	15	5
atsz–74a	Atlantic Source Zone	-82.7104	16.7695	82.35	15	17.94
atsz–74b	Atlantic Source Zone	-82.7709	17.1995	82.35	15	5
atsz–75a	Atlantic Source Zone	-81.7297	16.9003	79.86	15	17.94
atsz–75b	Atlantic Source Zone	-81.8097	17.3274	79.86	15	5
atsz–76a	Atlantic Source Zone	-80.9196	16.9495	82.95	15	17.94
atsz–76b	Atlantic Source Zone	-80.9754	17.3801	82.95	15	5
atsz–77a	Atlantic Source Zone	-79.8086	17.2357	67.95	15	17.94
atsz–77b	Atlantic Source Zone	-79.9795	17.6378	67.95	15	5
atsz–78a	Atlantic Source Zone	-79.0245	17.5415	73.61	15	17.94
atsz–78b	Atlantic Source Zone	-79.1532	17.9577	73.61	15	5
atsz–79a	Atlantic Source Zone	-78.4122	17.5689	94.07	15	17.94
atsz–79b	Atlantic Source Zone	-78.3798	18.0017	94.07	15	5
atsz–80a	Atlantic Source Zone	-77.6403	17.4391	103.3	15	17.94
atsz–80b	Atlantic Source Zone	-77.5352	17.8613	103.3	15	5
atsz–81a	Atlantic Source Zone	-76.6376	17.2984	98.21	15	17.94
atsz–81b	Atlantic Source Zone	-76.5726	17.7278	98.21	15	5
atsz–82a	Atlantic Source Zone	-75.7299	19.0217	260.1	15	17.94
atsz–82b	Atlantic Source Zone	-75.6516	18.5942	260.1	15	5
atsz–83a	Atlantic Source Zone	-74.8351	19.2911	260.8	15	17.94
atsz–83b	Atlantic Source Zone	-74.7621	18.8628	260.8	15	5
atsz–84a	Atlantic Source Zone	-73.6639	19.2991	274.8	15	17.94

Continued on next page

Table 5 – continued from previous page

Segment	Description	Longitude(°E)	Latitude(°N)	Strike(°)	Dip(°)	Depth (km)
atsz–84b	Atlantic Source Zone	-73.7026	18.8668	274.8	15	5
atsz–85a	Atlantic Source Zone	-72.8198	19.2019	270.6	15	17.94
atsz–85b	Atlantic Source Zone	-72.8246	18.7681	270.6	15	5
atsz–86a	Atlantic Source Zone	-71.9143	19.1477	269.1	15	17.94
atsz–86b	Atlantic Source Zone	-71.9068	18.7139	269.1	15	5
atsz–87a	Atlantic Source Zone	-70.4738	18.8821	304.5	15	17.94
atsz–87b	Atlantic Source Zone	-70.7329	18.5245	304.5	15	5
atsz–88a	Atlantic Source Zone	-69.7710	18.3902	308.9	15	17.94
atsz–88b	Atlantic Source Zone	-70.0547	18.0504	308.4	15	5
atsz–89a	Atlantic Source Zone	-69.2635	18.2099	283.9	15	17.94
atsz–89b	Atlantic Source Zone	-69.3728	17.7887	283.9	15	5
atsz–90a	Atlantic Source Zone	-68.5059	18.1443	272.9	15	17.94
atsz–90b	Atlantic Source Zone	-68.5284	17.7110	272.9	15	5
atsz–91a	Atlantic Source Zone	-67.6428	18.1438	267.8	15	17.94
atsz–91b	Atlantic Source Zone	-67.6256	17.7103	267.8	15	5
atsz–92a	Atlantic Source Zone	-66.8261	18.2536	262	15	17.94
atsz–92b	Atlantic Source Zone	-66.7627	17.8240	262	15	5

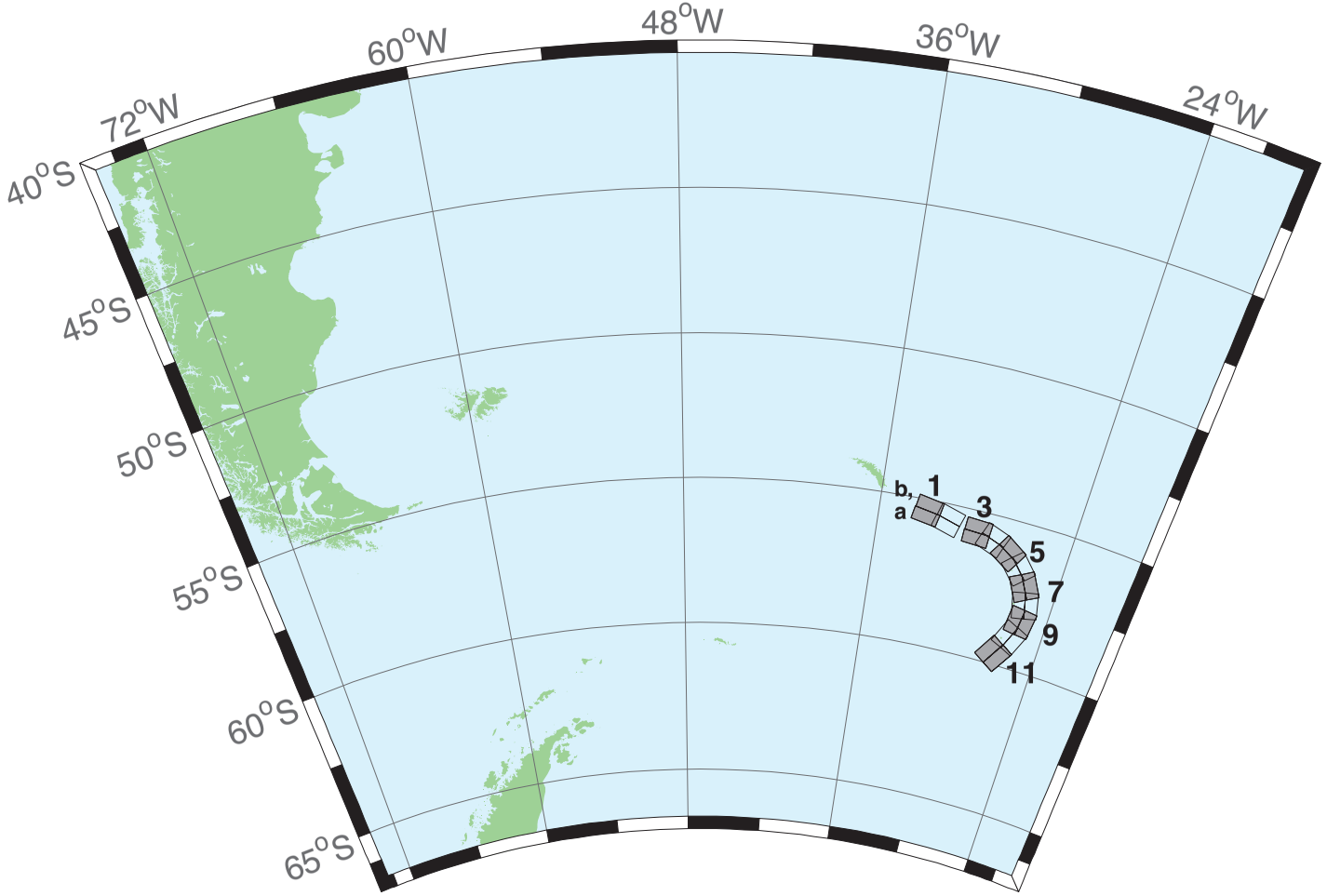

Figure 34: South Sandwich Islands Subduction Zone.

Table 6: Earthquake parameters for South Sandwich Islands Subduction Zone unit sources.

Segment	Description	Longitude(°E)	Latitude(°N)	Strike(°)	Dip(°)	Depth (km)
sssz–1a	South Sandwich Islands Subduction Zone	-33.0670	-55.3780	280.2	15	17.94
sssz–1b	South Sandwich Islands Subduction Zone	-32.9242	-54.9510	280.2	15	5
sssz–2a	South Sandwich Islands Subduction Zone	-31.7197	-55.5621	286.3	15	17.94
sssz–2b	South Sandwich Islands Subduction Zone	-31.4969	-55.1457	286.3	15	5
sssz–3a	South Sandwich Islands Subduction Zone	-29.8355	-55.7456	273	15	17.94
sssz–3b	South Sandwich Islands Subduction Zone	-29.7873	-55.3123	273	15	5
sssz–4a	South Sandwich Islands Subduction Zone	-28.7648	-55.8715	290	15	17.94
sssz–4b	South Sandwich Islands Subduction Zone	-28.4930	-55.4638	290	15	5
sssz–5a	South Sandwich Islands Subduction Zone	-27.6356	-56.1844	301.5	15	17.94
sssz–5b	South Sandwich Islands Subduction Zone	-27.2218	-55.8143	301.5	15	5
sssz–6a	South Sandwich Islands Subduction Zone	-26.7655	-56.5959	317.5	15	17.94
sssz–6b	South Sandwich Islands Subduction Zone	-26.1774	-56.3029	317.5	15	5
sssz–7a	South Sandwich Islands Subduction Zone	-26.0921	-57.1441	332.1	15	17.94
sssz–7b	South Sandwich Islands Subduction Zone	-25.3776	-56.9411	332.1	15	5
sssz–8a	South Sandwich Islands Subduction Zone	-25.7129	-57.7563	347.9	15	17.94
sssz–8b	South Sandwich Islands Subduction Zone	-24.9088	-57.6652	347.9	15	5
sssz–9a	South Sandwich Islands Subduction Zone	-25.7003	-58.3505	7.182	15	17.94
sssz–9b	South Sandwich Islands Subduction Zone	-24.8687	-58.4047	7.182	15	5
sssz–10a	South Sandwich Islands Subduction Zone	-26.0673	-58.9577	24.25	15	17.94
sssz–10b	South Sandwich Islands Subduction Zone	-25.2869	-59.1359	24.25	15	5
sssz–11a	South Sandwich Islands Subduction Zone	-26.8279	-59.6329	32.7	15	17.94
sssz–11b	South Sandwich Islands Subduction Zone	-26.0913	-59.8673	32.7	15	5

C SIFT Testing

By Lindsey Wright and Elena Tolkova

C.1 PURPOSE

Forecast models are tested with synthetic tsunami events covering a range of tsunami source locations and magnitudes. Testing is also done with selected historical tsunami events when available.

The testing of a forecast model has three objectives. The first objective is to assure that the results obtained with the NOAAs tsunami forecast system software, which has been released to the Tsunami Warning Centers for operational use, are consistent with those obtained by the researcher during the development of the forecast model. The second objective is to test the forecast model for consistency, accuracy, time efficiency, and quality of results over a range of possible tsunami locations and magnitudes. The third objective is to identify bugs and issues in need of resolution by the researcher who developed the Forecast Model or by the forecast system software development team before the next version release to NOAAs two Tsunami Warning Centers.

Local hardware and software applications, and tools familiar to the researcher(s), are used to run the Method of Splitting Tsunamis (MOST) model during the forecast model development. The test results presented in this report lend confidence that the model performs as developed and produces the same results when initiated within the forecast system application in an operational setting as those produced by the researcher during the forecast model development. The test results assure those who rely on the Savannah tsunami forecast model that consistent results are produced irrespective of system.

C.2 TESTING PROCEDURE

The general procedure for forecast model testing is to run a set of synthetic tsunami scenarios and a selected set of historical tsunami events through the forecast system application and compare the results with those obtained by the researcher during the forecast model development and presented in the Tsunami Forecast Model Report. Specific steps taken to test the model include:

- Identification of testing scenarios, including the standard set of synthetic events, appropriate historical events, and customized synthetic scenarios that may have been used by the researcher(s) in developing the forecast model.
- Creation of new events to represent customized synthetic scenarios used by the researcher(s) in developing the forecast model, if any.
- Submission of test model runs with the forecast system, and export of the results from A, B, and C grids, along with time series.
- Recording applicable metadata, including the specific forecast system version used for testing.
- Examination of forecast model results for instabilities in both time series and plot results.

- Comparison of forecast model results obtained through the forecast system with those obtained during the forecast model development.
- Summarization of results with specific mention of quality, consistency, and time efficiency.
- Reporting of issues identified to modeler and forecast system software development team.
- Retesting the forecast models in the forecast system when reported issues have been addressed or explained.

Synthetic model runs were tested on a DELL PowerEdge R510 computer equipped with two Xeon E5670 processors at 2.93 Ghz, each with 12 MBytes of cache and 32GB memory. The processors are hex core and support hyperthreading, resulting in the computer performing as a 24 processor core machine. Additionally, the testing computer supports 10 Gigabit Ethernet for fast network connections. This computer configuration is similar or the same as the configurations of the computers installed at the Tsunami Warning Centers so the compute times should only vary slightly.

C.3 Results

The Savannah forecast model was tested with SIFT version 3.2.

The Savannah, Georgia forecast model was tested with three synthetic scenarios. Test results from the forecast system and comparisons with the results obtained during the forecast model development are shown numerically in Table 1 and graphically in Figures 35 to 37. The results show that the minimum and maximum amplitudes and time series obtained from the forecast system agree with those obtained during the forecast model development, and that the forecast model is stable and robust, with consistent and high quality results across geographically distributed tsunami sources. The model run time (wall clock time) was 12.40 minutes for 11.99 hours of simulation time, and 4.12 minutes for 4.0 hours. This run time is well within the 10 minute run time for 4 hours of simulation time.

A suite of three synthetic events was run on the Savannah forecast model. A slip of 30 m was used for the South Sandwich (SSSZ 1-10) scenario rather than the standard 25m for direct comparison purposes. The modeled scenarios were stable for all cases run. The largest modeled height was 114 centimeters (cm) from the Atlantic (ATSZ 48-57) source zone. The smallest signal of 22.9 cm was recorded at the South Sandwich (SSSZ 1-10) source zone. Visual comparisons between the development cases and the forecast system output were nearly identical in shape and amplitude for all cases. The Savannah reference point used for the forecast model development is the same as what is deployed in the forecast system, so the results can be considered valid for the three cases studied.

Scenario Name	Source Zone	Tsunami Source	α (m)	SIFT Max (cm)	Development Max (cm)	SIFT Min (cm)	Development Min (cm)
ATSZ 35-44*	Atlantic	A35-44, B35-44	25	35.4	47.7	-26.8	-32.3
ATSZ 48-57*	Atlantic	A48-57, B48-57	25	114.1	117.3	-111.7	-99.5
SSSZ 1-10*	South Sandwich	A1-10, B1-10	30	22.9	31.8	-26.2	-34.3

Table 7: Table of maximum and minimum amplitudes at Savannah, Georgia warning point for synthetic and historical events tested using SIFT.

*Some difference between the testing results and the results obtained during the model development is due to an update of the propagation database, which resulted in using slightly different synthetic scenarios for development and for testing.

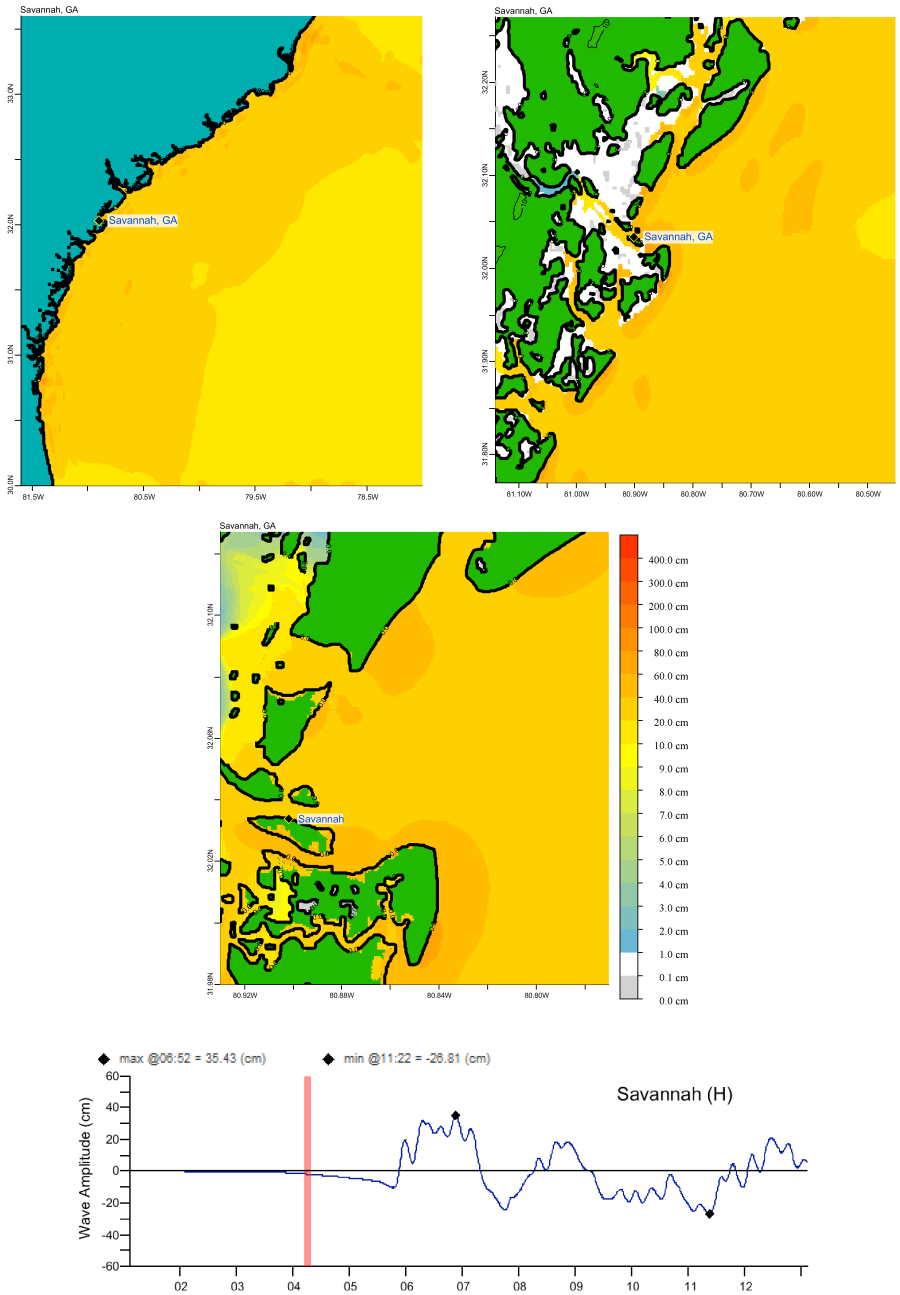

Figure 35: Response of the Savannah forecast model to synthetic scenario ATSZ 35-44 (alpha=25). Maximum sea surface elevation for A-grid (top left), B-grid (top right), C-grid (center). Sea surface elevation time series at the C-grid warning point (bottom), to be compared with the black curve in Figure 16.

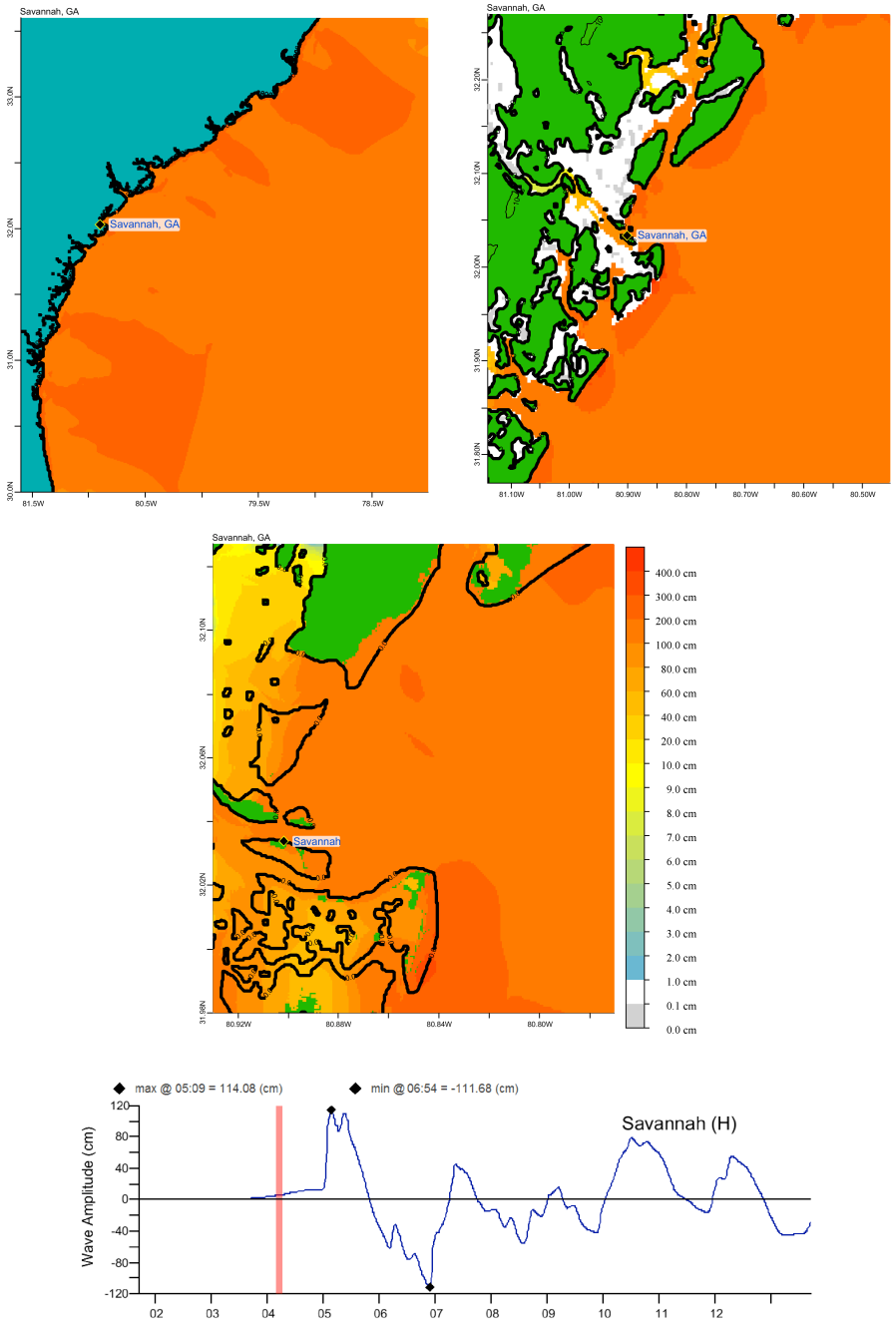

Figure 36: Response of the Savannah forecast model to synthetic scenario ATSZ 48-57 (alpha=25). Maximum sea surface elevation for A-grid (top left), B-grid (top right), C-grid (center). Sea surface elevation time series at the C-grid warning point (bottom), to be compared with the black curve in Figure 18.

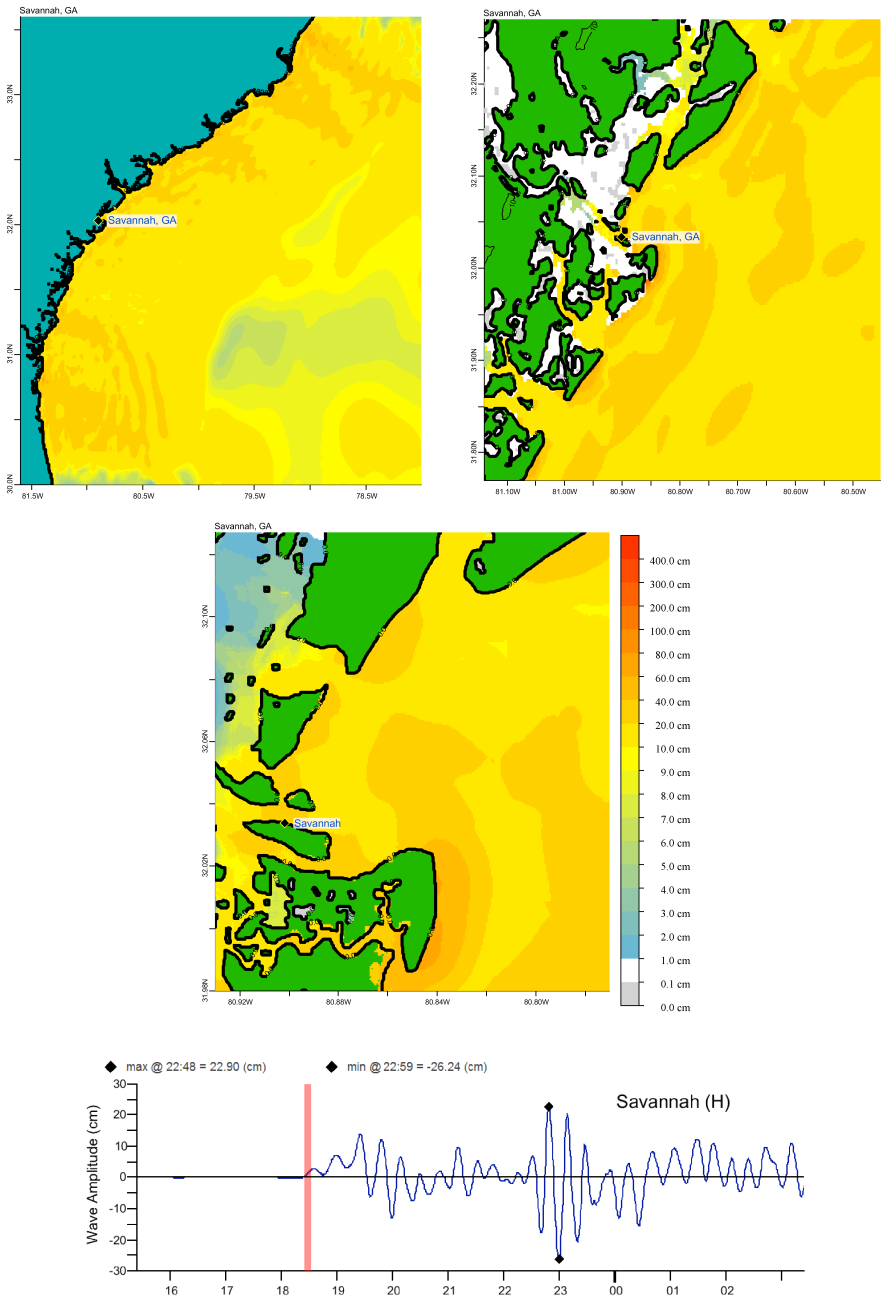

Figure 37: Response of the Savannah forecast model to synthetic scenario SSSZ 1-10 (alpha=30). Maximum sea surface elevation for A-grid (top left), B-grid (top right), C-grid (center). Sea surface elevation time series at the C-grid warning point (bottom), to be compared with the black curve in Figure 24.